Frontal Cortex Hyperactivation and Gamma Desynchrony in Fragile X Syndrome: Correlates of Auditory Hypersensitivity

Authors: Ernest V. Pedapati[1,2,3¶], Lauren E. Ethridge[6,7¶], Yanchen Liu[1], Rui Liu[1], John A. Sweeney[3], Lisa A. DeStefano[4], Makoto Miyakoshi[1], Khaleel Razak[11], Lauren M. Schmitt[4,5], David R. Moore[9,10], Donald L. Gilbert[2,5], Steve W. Wu[2,5], Elizabeth Smith[4,5], Rebecca C. Shaffer[4,5], Kelli C. Dominick[1,3], Paul S. Horn[2], Devin Binder[8], and Craig A. Erickson[1,3]

¶These authors contributed equally to this work.

Affiliations:

[1]Division of Child and Adolescent Psychiatry, Cincinnati Children's Hospital Medical Center, Cincinnati, OH, United States.

[2]Division of Neurology, Cincinnati Children's Hospital Medical Center, Cincinnati, OH, United States.

[3]Department of Psychiatry, University of Cincinnati College of Medicine, Cincinnati, OH, United States.

[4]Division of Developmental and Behavioral Pediatrics, Cincinnati Children's Hospital Medical Center, Cincinnati, OH, United States.

[5]Department of Pediatrics, University of Cincinnati College of Medicine, Cincinnati, OH, United States.

[6]Department of Pediatrics, Section on Developmental and Behavioral Pediatrics, University of Oklahoma Health Sciences Center, Oklahoma City, OK, United States.

[7]Department of Psychology, University of Oklahoma, Norman, OK, United States.

[8]Division of Biomedical Sciences, School of Medicine, University of California, Riverside, United States.

[9]Communication Sciences Research Center, Cincinnati Children's Hospital Medical Center, Cincinnati, OH, United States.

[10]Manchester Centre for Audiology and Deafness, University of Manchester, Manchester, UK

[11]Department of Psychology, University of California, Riverside, Riverside, CA, United States.

*Corresponding author: Ernest Pedapati

E-mail: ernest.pedapati@cchmc.org (EP)

Abstract

Fragile X syndrome (FXS) is an X-linked disorder that often leads to intellectual disability, anxiety, and sensory hypersensitivity. While sound sensitivity (hyperacusis) is a distressing symptom in FXS, its neural basis is not well understood. It is postulated that hyperacusis may stem from temporal lobe hyperexcitability or dysregulation in top-down modulation. Studying the neural mechanisms underlying sound sensitivity in FXS using scalp electroencephalography (EEG) is challenging because the temporal and frontal regions have overlapping neural projections that are difficult to differentiate. To overcome this challenge, we conducted EEG source analysis on a group of 36 individuals with FXS and 39 matched healthy controls. Our goal was to characterize the spatial and temporal properties of the response to an auditory chirp stimulus. Our results showed that males with FXS exhibit excessive activation in the frontal cortex in response to the stimulus onset, which may reflect changes in top-down modulation of auditory processing. Additionally, during the chirp stimulus, individuals with FXS demonstrated a reduction in typical gamma phase synchrony, along with an increase in asynchronous gamma power, across multiple regions, most strongly in temporal cortex. Consistent with these findings, we observed a decrease in the signal-to-noise ratio, estimated by the ratio of synchronous to asynchronous gamma activity, in individuals with FXS. Furthermore, this ratio was highly correlated with performance in an auditory attention task. Compared to controls, males with FXS demonstrated elevated bidirectional frontotemporal information flow at chirp onset. The evidence indicates that both temporal lobe hyperexcitability and disruptions in top-down regulation play a role in auditory sensitivity disturbances in FXS. These findings have the potential to guide the development of therapeutic targets and back-translation strategies.

Introduction

Fragile X Syndrome (FXS) is an X-linked neurodevelopmental disorder caused by methylation-based silencing of fragile X messenger ribonucleoprotein (FMRP)[1]. Individuals with FXS typically experience intellectual disability, anxiety, and sensory hypersensitivity, specifically hyperacusis, which is an increased sensitivity to sounds. Auditory hypersensitivity can have a significant impact on daily functioning and may present as difficulty tolerating certain sounds, heightened sensitivity to loud noises, and an overall increased sensitivity to auditory stimuli[2]. Studies using electroencephalography (EEG) have provided insight into the temporal abnormalities of auditory processing in FXS[3–5]. However, it remains poorly understood how different regions of the brain contribute to hyperacusis in FXS[6].

Interrogation of the auditory system using the chirp stimulus (broadband noise amplitude modulated by a sinusoid linearly increasing in frequency from 0-100 Hz over 2 seconds) is a valuable method to examine neural synchronization and background response across a range of frequencies, typically leading to phase alignment within the gamma frequency range (30-80 Hz) [7]. This precise phase alignment of gamma oscillations contributes to sensory and higher-order processes [8,9]. Gamma oscillations that are locked to stimuli play an important role in filtering and amplifying the processing of sensory stimuli [10,11]. Alternatively, it is hypothesized that increases in asynchronous gamma activity could be considered “noise” that may interfere with or reduce the auditory cortex’s ability to contextually modulate and precisely align gamma oscillations to task demands.

Auditory evoked potential (AEP) studies in FXS have reproducibly demonstrated impairments in gamma phase synchronization and elevations in background gamma power when using the chirp stimulus [12–14]. These alterations were correlated with cognitive measures including auditory attention, processing speed, and cognitive flexibility[14]. Indeed, in FXS, in addition to gamma phase synchrony deficits, asynchronous elevations in gamma power have

been observed at rest [15–18], during speech tasks[19], and in during auditory tasks [12,14]. These similar alterations in gamma synchronization and asynchronous gamma power can be observed in *Fmr1*$^{-/-}$ KO mouse which is the primary animal model for FXS[20,21]. Given that FMRP regulates synapses in an activity- and stimulus-dependent manner, it can be hypothesized that the absence or reduction of FMRP impairs the precision and efficiency of neural firing, particularly in regions and networks that experience high cognitive or sensory processing demands[22,23].

Recent studies, including those conducted in ASD, have found that conditioned top-down activity originating in the frontal cortex provides contextual cues to modulate auditory system sensitivity[24–28]. However, the specific contribution of different brain regions to auditory hypersensitivity in FXS remains unclear. This is primarily due to limitations of EEG analysis at the scalp level, which may not accurately reflect auditory cortex activity due to its tangential overlap with frontal sources[29]. By examining the spatial distribution of gamma abnormalities during the auditory chirp, we can enhance our understanding of the anatomical origins of sensory dysfunction in FXS and establish systems-level correlates with phenotype[3–5,30].

In this study, we examined source-localized EEG responses to the auditory chirp to characterize spatial and time-domain characteristics of primarily gamma band synchronization and background power. We conducted the study in a well-powered sample of individuals with FXS as well as sex- and age-matched typically developing controls. Our hypothesis was that individuals with FXS would exhibit chirp-associated phase locking deficits, primarily localized to the temporal regions. This was based on the understanding that frequency-following response typically reflects basic bottom-up sensory processing from subcortical and sensory cortical sources[31]. Additionally, we hypothesized that the onset of the chirp stimulus, which engages contextual cueing and salience processing, would elicit a strong response in the frontal cortex[32]. As thalamocortical dysrhythmia is implicated in Fragile X syndrome, likely contributing to atypical neural oscillations, we examine alpha oscillations as possible markers of such deeper disruptions

in thalamocortical circuitry and known neuroimaging abnormalities across the cingulate cortex, amygdala, inferior colliculus, and other subcortical structures[33]. Furthermore, we expected to observe sex differences in individuals with FXS, consistent with varying levels of FMRP expression[33]. Finally, we predicted that these neurophysiological alterations would be associated with neurocognitive and behavioral correlates, particularly impairments in an auditory attention task that incorporates both top-down and sensory aspects.

Materials and Methods

Participants

A methodological overview of the study procedures is depicted in **Figure 1**. Thirty-six participants with FXS (23 males; age, 10-53 years; mean age, 25.4±10.3 years) and 39 age- and sex-matched typically developing controls (22 males; age, 12-57 years; mean age, 28.0±12.2 years) participated in this study (**see Table 1**). The age and proportion of each sex did not differ between groups. Scalp-level electrode analyses of this dataset were previously published[14]. In our study, all participants gave written informed consent. For minors aged 11 to 17, both the child/teen provided assent and a parent or guardian provided written consent. No waivers for parental consent were granted by the IRB. All procedures were approved by the Cincinnati Children's Hospital Institutional Board (IRB 2015-8425). Recruitment for the study occurred under NIH FXS Center (U54HD082008) grant began on 1/18/2016 and completed 5/31/2020. Typically developing control (TDC) participants were screened for prior diagnosis or treatment for neuropsychiatric illness, hearing loss, psychiatric medication use, or first-degree relatives affected by serious psychiatric or neurodevelopmental disorders. Participants with FXS were excluded if they had a history of hearing impairment, epilepsy, or recent administration of anticonvulsant medications (including benzodiazepines) that could confound EEG interpretation. To ensure a representative sample of the FXS population[34], participants on stable doses (at least four weeks) of psychiatric medicines were permitted.

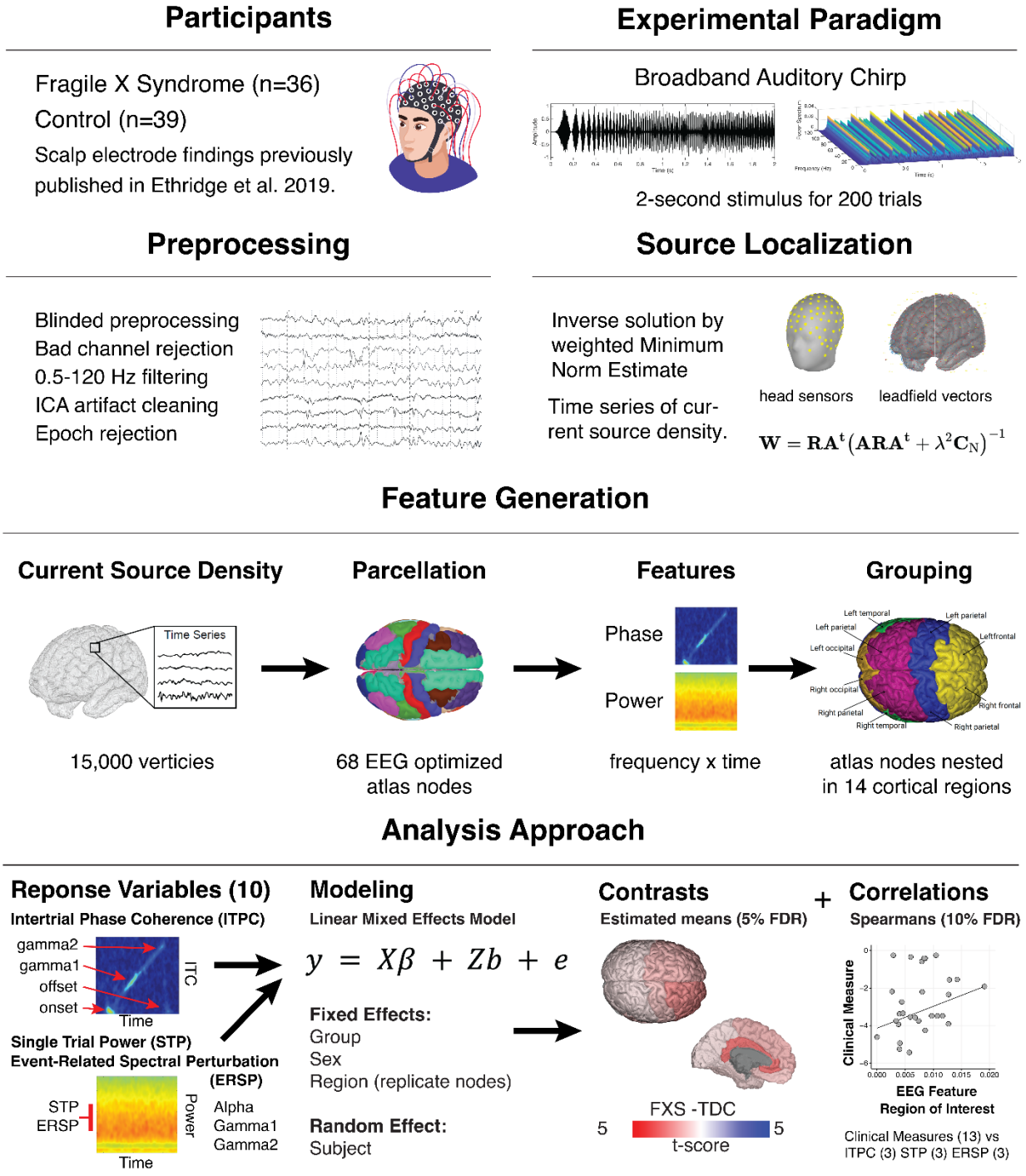

Figure 1. Overview of the principal methodology. An auditory evoked potential case-control study using dense array EEG, source localization, and advanced statistical modeling to identify spatiotemporal neural responses to the chirp stimuli and clinical correlations.

	Group		
Measure	FXS, N = 36[1]	TDC, N = 39[1]	p-value[2]
Sex			.5
F	13 (36%)	17 (44%)	
M	23 (64%)	22 (56%)	
Age at Visit	25.4±10.3	28.0±12.2	.5
Deviation IQ	42.4±29.1	102.9±8.3	<.001
NVIQ	31.9±36.1	103.6±11.2	<.001
VIQ	54.9±28.3	102.3±1.8	<.001
ADAMS General Anxiety	7.7±4.8	2.4±2.6	<.001
ADAMS Obsessive/Compliance Behavior	2.4±2.3	.5±1.3	<.001
SCQ Total	14.0±7.9	2.2±2.4	<.001
ABC FXS subscale 1: Irritability/aggression	11.2±11.4	.6±2.4	<.001
ABC FXS subscale 4: Hyperactivity/Noncompliance	7.7±5.9	.9±2.1	<.001
ABC FXS subscale 5: Inappropriate speech	4.4±3.5	.2±.6	<.001
ABC FXS subscale 2: lethargy/social withdrawal	5.5±4.4	.6±1.5	<.001
ABC FXS subscale 3: stereotypy	4.0±4.5	.1±.4	<.001
WJ3	65.2±17.9	91.9±11.7	<.001

[1]n (%); Mean±SD

[2]Pearson's Chi-squared test; Wilcoxon rank-sum test

Table 1. Demographics and clinical features of study participants by group. Abbreviations: FXS, Fragile X Syndrome; TDC, typically developing control; F, female; M, male; NVIQ, Non-verbal intelligence quotient; VIQ, verbal intelligence quotient; SCQ, Social Communication Questionnaire; ABC, Aberrant Behavior Checklist; WJ-3, Woodcock III Tests of Cognitive Abilities; ADAMS, Anxiety, Depression, and Mood Scale.

Psychological measures

Participants' cognitive abilities (IQ) were estimated using the Stanford-Binet Intelligence Scales 5th Ed. Abbreviated IQ test. To account for floor effects, deviation scores were calculated for verbal and non-verbal IQ in lower ranges[35]. Selective speech-sound discrimination was measured in participants using the Woodcock-Johnson III Tests of Cognitive Abilities Auditory Attention (WJ3)[36]. Caregiver assessments of FXS participants included the Social and Communication Questionnaire (SCQ), Anxiety Depression and Mood Scale (ADAMS)[37], and Aberrant Behavior Checklist-Community (ABC-C, optimized for FXS)[38].

Experimental stimulus

Auditory stimuli were presented diotically through Sony MDR-V150 headphones (65 dB SPL RMS) using Presentation 22 (Neurobehavioral Systems) in a sound-attenuated room. Participants viewed a silent video during the task to facilitate protocol compliance and promote quiet wakefulness[13,15].

An auditory chirp stimulus was employed to evaluate the integrity of functional cortical responses[7]. The stimulus consisted of a pink noise carrier that is amplitude modulated by a sinusoid linear chirp which increased in frequency from 0 to 100 Hz over 2000 ms (Supplemental Figure 1A-1B). Participants were presented with 200 repetitions, with each repetition having an interstimulus interval randomly varied between 1500 and 2000 milliseconds. Cortical responses to the chirp were measured using intertrial phase coherence (ITPC), which indicates the strength and consistency of neural phase locking to the stimulus. Control participants typically demonstrate a strong attunement to the current frequency of the chirp, as evidenced by high ITPC values across the frequency range of the chirp[7].

EEG acquisition and preprocessing

EEG was continuously recorded and referenced to Cz with a sampling rate of 1000 Hz using a NetAmp 400 (Magstim/EGI, Eugene, Oregon) with a Hydrocel 128-channel geodesic saline-based electrode net. Raw data were deidentified and visually inspected offline. Data were digitally filtered from 0.5-120 Hz (12 and 24 dB/octave roll-off, respectively; zero-phase; 60 Hz notch). Bad sensors were interpolated (up to 5% per subject, no more than two adjacent sensors) using spherical spline interpolation implemented in BESA 6.1 (MEGIS Software, Grafelfing, Germany). Ocular, cardiac, and muscle movement artifacts were removed blind to participant group status using independent components analysis (extended infomax) implemented in EEGLAB[39] using MATLAB 2021a (MathWorks, Natick, MA). Segments of data with large movement artifacts were removed before ICA to facilitate algorithm convergence. Data were then transformed to average reference and segmented into 3250 ms trials (-500 ms to 2750 ms). Any trial with post-ICA amplitude exceeding 120 μV was considered as containing residual artifact and removed.

EEG analyses

Source localization

A depth-weighted minimum norm estimate (MNE) model in Brainstorm was used to estimate a distributed source model[40]. Several methods have been developed to calculate dipolar magnitudes from scalp potentials and electrode positions[41]. MNE identifies a solution that minimizes the influence of total brain power and corresponds to Tikhonov regularization[42]. To account for the bias of weaker surface sources towards electrodes in the classical MNE solution, a depth weighting (order, .5; maximal amount, 10) was applied to normalize source amplitude values[43]. The model was constrained to dipoles normal to the cortical surface to optimize for dense array EEG analysis, and an identity matrix was used for noise covariance.

Scalp electrodes were co-registered to the ICBM152 common brain template[44]. The forward model, or lead field matrix, was computed using Open MEEG resulting in a boundary element method head model that accounts for the brain, CSF, skin, and skull conductivity properties[45]. An MNE kernel was then implemented to generate a current source density (CSD) time series across a resultant triangular mesh (15,002 vertices) representing the cortical envelope. The vertices were parcellated into 68 cortical nodes (Nodes) according to the Desikan-Killiany (DK) atlas[46]. The DK atlas includes fourteen hierarchical anatomical grouping variables combining information across cortical regions (**see Supplemental Figure 2**). The temporal lobe region included homologous right and left pairs of the following nodes: banks of the superior temporal sulcus and transverse temporal gyrus, which are on or adjacent to AC.

Time-frequency analyses

For each DK atlas node, waveforms were analyzed using the *newtimef* function included with EEGLAB 2021. Convolution parameters included using Morlet wavelets with one Hz frequency steps using a linearly increasing cycle length from one cycle at the lowest frequency (2 Hz) to 30 cycles at the highest frequency (120 Hz). For any segmented amplitude time series and frequency step, *newtimef* function generates mean ITPC (aka phase locking value or intertrial coherence), single-trial power (STP), and event-related spectral perturbation (ERSP). A total of ten phase and power variables were generated for each subject per atlas node to account for the frequency band and time point (see below).

Phase measures

ITPC was examined at predefined time points corresponding to chirp frequency intervals as follows: onset (2-13 Hz), gamma1 (30-57 Hz), and gamma2 (63-100 Hz). Offset ITPC was evaluated at 2-13 Hz. ITPC estimates the degree of phase-locked responses across trials; however, it can be biased by trial number. To avoid bias, raw ITPC values were corrected for trial numbers by subtracting the critical r value according to the following equations[13]:

Eq. 1 $$r_{critical} = \sqrt{\frac{-1}{trial\ count * \ loglog\ (.5)}}$$

Eq. 2 $$ITPC_{corrected} = ITPC_{raw} - r_{critical}$$

Power measures

Trial-level STP and ERSP were computed across alpha (8-12 Hz), gamma1, and gamma2 frequencies to be comparable with previous scalp electrode findings[13,14]. STP measures the spectral power of the frequency response, while ERSP quantifies the change in spectral power by frequency corrected for the pre-stimulus baseline (-500 to 0 ms).

Effective connectivity

Transfer entropy (TE) was used to study targeted directional interactions to investigate causal relationships between frontal and temporal sources. TE is an information theory-based effective connectivity measure suitable for identifying non-linear interactions and is robust to volume conduction[47]. The estimation of TE was implemented using the RTransferEntropy[48] package in R4.2. TE was based on Rényi entropy, an algorithm commonly used in neuroscience applications [49].

Eq. 3 $$RT_{J\to I}(k,l) = \frac{1}{1-q}\log\left(\frac{\sum_i \phi_q\left(i_t^{(k)}\right) p^q\left(i_{t+1} \mid i_t^{(k)}\right)}{\sum_{i,j} \phi_q\left(i_t^{(k)}, j_t^{(l)}\right) p^q\left(i_{t+1} \mid i_t^{(k)}, j_t^{(l)}\right)}\right)$$

Pairs of artifact-free node-level epoched time series (60 trials) were used as X and Y input vectors, with the default Markov order of 3 for k and 3. To assess the statistical significance of TE, the Markov block bootstrap method (300 replications) was employed to preserve the dependencies within each time series under the null hypothesis of no information transfer[50]. A maximum p-value of $p \leq 0.01$ was considered significant for a connection. The empirical distribution of the time series was discretized into 5% and 95% quantiles. After estimating TE, the percentage of trials that exhibited a significant TE connection was calculated for each subject in order to facilitate group comparison.

241

242 ## Statistical analyses

243 ### Linear modeling

244 All statistical analyses were performed in R (version 4.2). To account for individual
245 variation in electrode position, we opted to perform statistical modeling at the region level and use
246 nodes within a DK region as replicates (Supplemental Table 1). We conducted a series of linear
247 mixed-effects models (LME) for each of the ten response variables (see Phase and Power
248 measures) using the NLME library with the general form:

249 Eq. 4 $$y = X\beta + Zb + e$$

250 Where y is the response variable, X is the design matrix for the fixed effect coefficients, β,
251 Z is the design matrix of random effects coefficient, b, and e is the vector of random errors.
252 Denominator degrees of freedom for each fixed effect (and required for conditional F-tests) are
253 estimated with NLME using the method described in Pinheiro and Bates[51]. Fixed effects
254 included Group (FXS or TDC), Sex (male or female), and Region (n=14; Supplemental Figure 2).
255 After examining various link functions, ITPC response variables were log-transformed and raised
256 to 1/3 power. This was validated using Akaike's information criterion (AIC), examining plots of the
257 distribution of the residuals, residuals over predicted values, and quantile-quantile plots. Based
258 on significant interactions, post-hoc contrasts between least-squared means (LSMEANS) were
259 conducted and corrected using a 5% false discovery rate (FDR)[52]. Cohen's d effect sizes (ES)
260 were calculated for pairwise comparisons. Though adjusted $p \leq .05$ was considered statistically
261 significant, adjusted $p < .10$ is presented along with ES to provide suggestive findings that may
262 be of heuristic interest. Clinical correlations: Spearman's ρ was used to estimate the association
263 between clinical measures and EEG response variables. We examined relationships across all
264 FXS participants for our primary correlation analysis and applied a 10% FDR correction. We also
265 explored uncorrected correlations within males with FXS.

Results

Alterations of intertrial phase coherence (ITPC) in FXS

Reduction in gamma band ITPC in FXS

Our findings indicate a disruption in gamma-band chirp frequency synchronization in FXS. Disruption was larger in males in the right temporal, right parietal, left prefrontal, and bilateral central regions (**see Figure 2A and Table 2**). A representative time-frequency plot of right temporal ITPC by group is shown in Figure 3A, with group differences in Figure 3B. For gamma1 ITPC, we found a significant interaction effect of group, sex, and region ($F_{13,4973}$=1.9, p < .001; see Figure 3C). For gamma2 ITPC, a two-way interaction between group and region was significant ($F_{13,4973}$=4.6, p < .001; see Figure 3D). Post-hoc comparisons found a significant reduction of gamma2 ITPC only in the left temporal cortex (LT: t_{71}=-4.4, p=<.001, adj. p=<.001), with a trend within the right temporal cortex (RT: t_{71}=-2.7, p=.009, adj. p=.065).

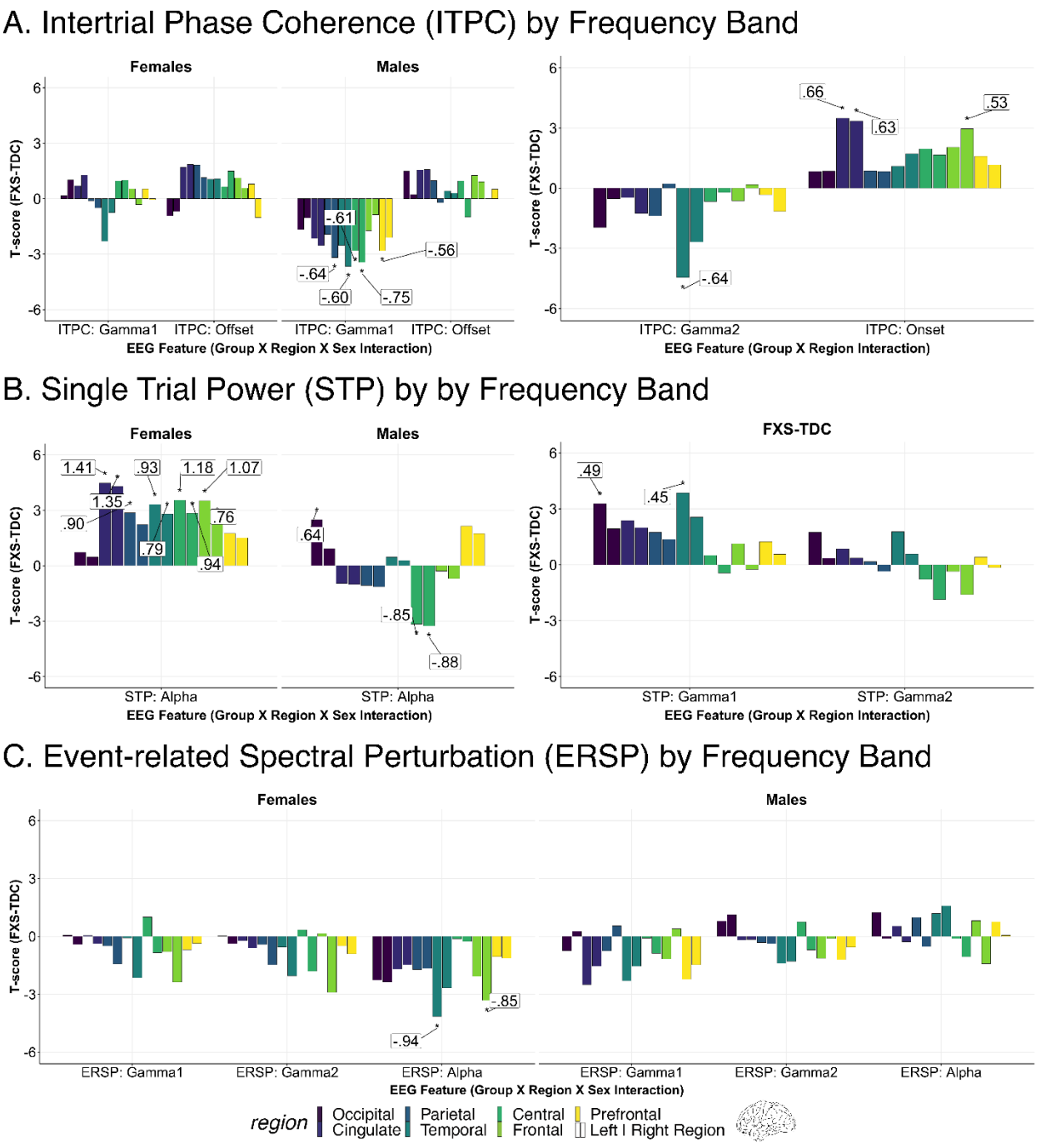

Figure 2. Altered neural responses to auditory chirp in Fragile X Syndrome (FXS). For each chirp-associated EEG feature, bar plots depict 5% FDR corrected post-hoc pairwise comparisons between groups of significant fixed or interaction effects (noted below the x-axis). Each significant bar (*) is annotated with the associated Cohen's *d* effect size. Each pair of bars represents brain regions corresponding to either left (left bar) or right (right bar) hemispheres.

Positive t-values indicate that the feature estimates in FXS are greater than in matched controls. A. Intertrial Phase Coherence (ITPC): Left: Males with FXS demonstrate impairment in gamma ITPC to the auditory chirp. Right: Individuals with FXS display increased onset ITPC to the auditory chirp compared to controls localized to frontal and cingulate regions. Cingulate regions in this EEG-optimized atlas primarily refer to cingulate cortical regions and other deeper sources. B. Single trial power (STP): Left: Alpha STP is increased in FXS females and reduced in FXS males compared to controls. Right: Individuals with FXS demonstrate heightened gamma STP in the left temporal and left occipital regions. Similar trend-level effects were found in the right temporal (p=.013, adj. p=.061) and left cingulate (p=.020, adj. p=.072) regions. C: Event-related spectral perturbation (ERSP): Left: Females with FXS demonstrated a significant (or trending) increase in alpha power across bilateral cortical regions. Right: A significant group x sex x region interaction for gamma1 ERSP ($p < .001$) and gamma2 ERSP ($p = .017$) was present, but no pairwise comparisons survived correction. A review of raw p values and effect sizes suggests the interaction was driven by decreased gamma1 ERSP in males with FXS.

Variable	Region	Sex	FXS	TDC	DF	F	ES	p	adj. p
ITPC: Gamma1	LC	M	.018±.027	.030±.031	71	-2.8	-.61	.006	.037
	LPF	M	.006±.013	.016±.018	71	-2.8	-.56	.007	.037
	LT	F	.016±.015	.028±.032	71	-2.3	-.46	.024	.085
	LT	M	.019±.032	.029±.037	71	-2.5	-.41	.014	.056
	RC	M	.018±.020	.036±.030	71	-3.4	-.75	<.001	.013
	RL	M	.033±.038	.045±.040	71	-2.5	-.51	.014	.056
	RP	M	.015±.020	.027±.022	71	-3.2	-.64	.002	.020
	RT	M	.017±.022	.033±.043	71	-3.7	-.60	<.001	.013
ITPC: Gamma2	LT		.008±.015	.016±.020	71	-4.4	-.64	<.001	<.001
	RT		.008±.010	.014±.020	71	-2.7	-.39	.009	.065
ITPC: Onset	LL		.105±.089	.064±.054	71	3.5	.66	<.001	.009
	RF		.074±.067	.047±.043	71	3.0	.53	.004	.019
	RL		.111±.090	.070±.055	71	3.4	.63	.001	.009

Table 2. Significant intertrial phase coherence (ITPC) contrasts by frequency band. Significant corrected linear mixed model post-hoc group contrasts of least-squared means (± standard error) of ITPC. Abbreviations: ES, Cohen's *d* effect size; adj. p, 5% false discovery rate corrected p values; FXS, Fragile X Syndrome; TDC, typically developing controls; DF, degrees of freedom; FDR, false discovery rate; LC, left central; RC, right central; LPF, left prefrontal; LT, left temporal; RT, right temporal; RL, right cingulate; LL, left cingulate; RP, right parietal.

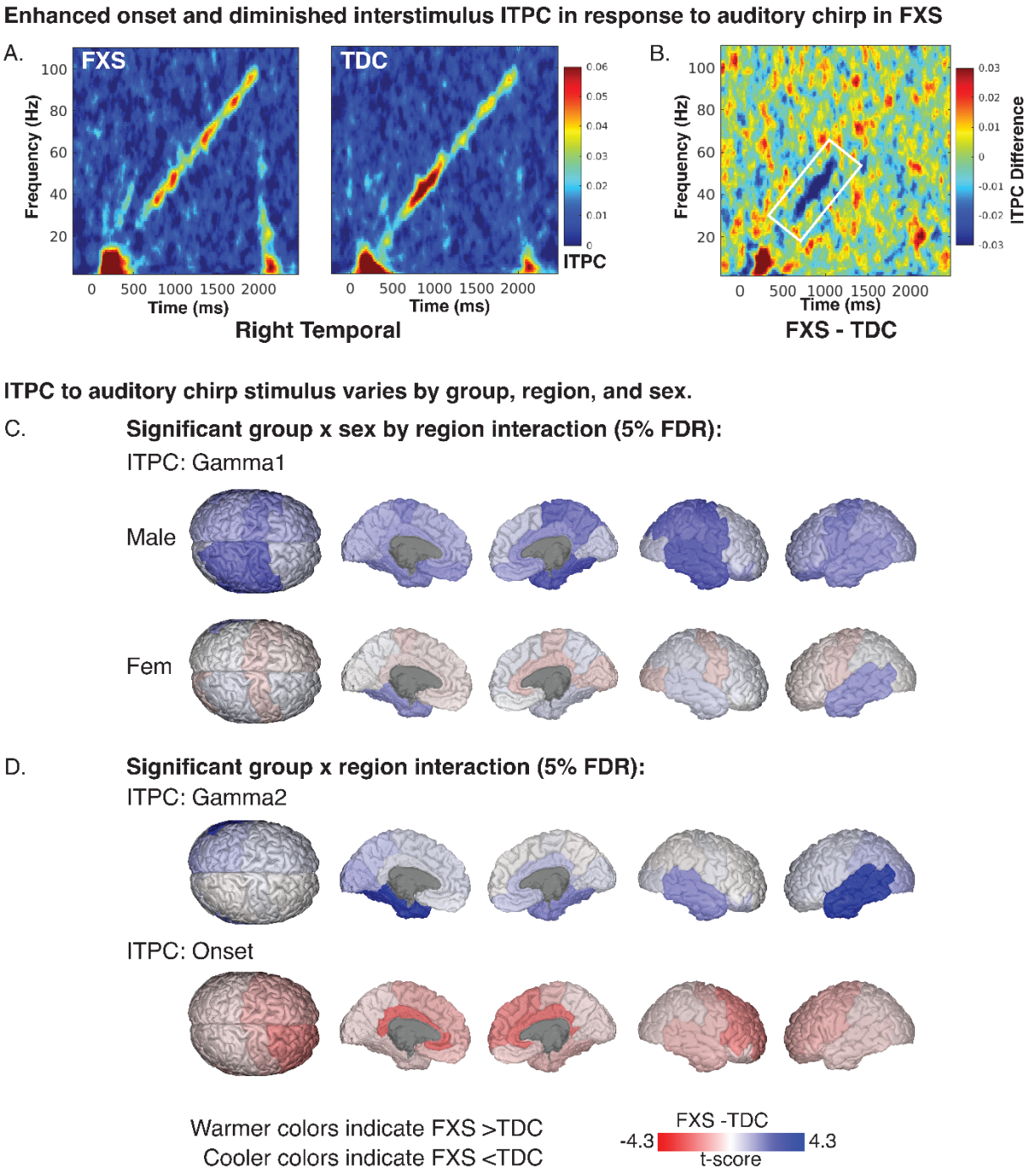

Figure 3. Intertrial phase coherence in response to auditory chirp. A. Time-frequency heatmaps for depicting mean ITPC response by group in the right temporal region. B. ITPC difference plot (FXS-TDC) with white outline marking a significant reduction of Gamma1 ITPC in

309 FXS. C. Brain plots depicting least-square means contrasts (t-values) of Gamma1 ITPC. D. Brain

310 plots depicting least-square means contrasts (t-values) of Gamma2 and onset ITPC.

Enhanced frontal onset ITPC in FXS

Onset ITPC to the chirp stimulus was increased in FXS (significant group by region interaction; $F_{13,4973}$=2.9, p < .001; **see Table 2**) within the right frontal (RF: t_{71}=3.0, p=.004, adj. p=.019), right cingulate (RL: t_{71}=3.4, p=.001, adj. p=.009), and left cingulate regions (LL: t_{71}=3.5, p=<.001, adj. p=.009; **see Figure 2A and 3D**). Due to the significant decline in the precision of EEG source localization at deeper depths, the cingulate area within the EEG-optimized DK atlas includes the cingulate cortex and other deep brain sources such as the inferior colliculus (**see Supplemental Table 1**) [30,53].

No offset ITPC differences were found across FXS and TDC

Although a significant interaction effect of group x sex x region was identified in the LME of offset ITPC ($F_{13,4973}$=1.7, p < .047; see Figure 2), no pairwise contrasts survived correction for multiple comparisons. The effect is likely driven by increased offset ITPC in the FXS group.

Alterations of Single Trial Power (STP)

Elevation in asynchronous gamma single-trial power.

Elevated background gamma STP has been detected at the scalp level in humans with FXS and Fmr1$^{-/-}$ KO studies at rest and in response to the auditory chirp [13,14,54,55]. Considering deficits in gamma ITPC in FXS, this background activity has been hypothesized to represent asynchronous background noise. For gamma1 and gamma2 STP, we predicted a significant increase in gamma STP in FXS within temporal regions with a larger effect in males. We found two significant, two-way interactions (group x sex and sex x region). Based on our a priori hypothesis, we examined pairwise contrasts for the significant group x region interaction effect (gamma1 STP: $F_{13,4973}$=2.6, p=.002; gamma2 STP: $F_{13,4973}$=2.5, p=.002). We identified significant and trend level increases in gamma STP in participants with FXS within the left temporal (LT: t_{71}=3.9, p=<.001, adj. p=.004), right temporal (RT: t_{71}=2.5, p=.013, adj. p=.061), left

cingulate (LL: t_{71}=2.4, p=.020, adj. p=.072), and left occipital regions (LO: t_{71}=3.3, p=.002, adj. p=.011) (see Figure 4E, 4F). A time-frequency plot of left temporal gamma1 STP contrasts by group is shown in Figure 4A with regional differences shown in Figure 4E. No gamma2 STP pairwise contrasts survived correction.

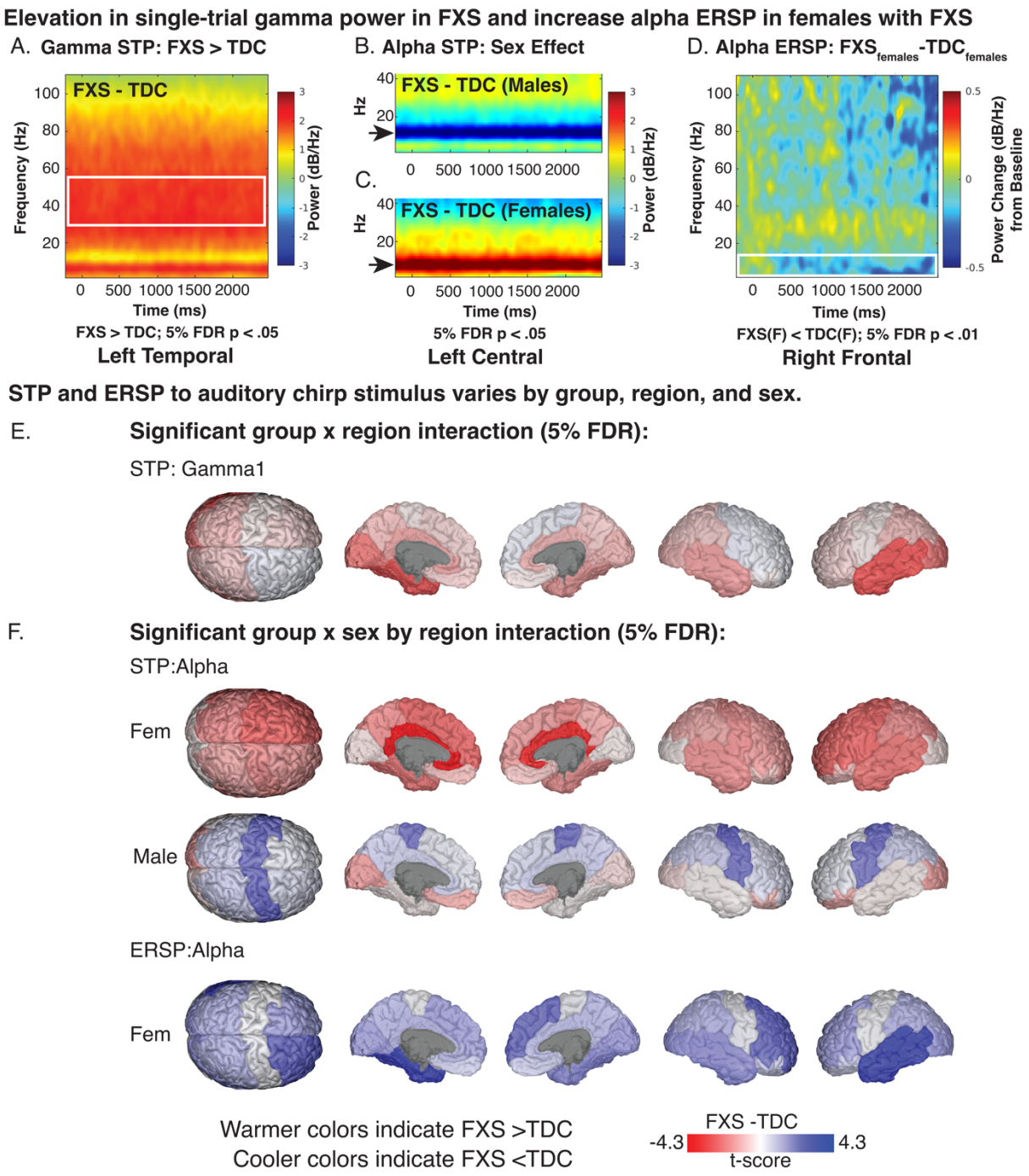

Figure 4. Single-trial power (STP) and event-related spectral perturbation (ERSP) in response to auditory chirp. A-D. Exemplar time frequency heatmaps visualizing STP and ERSP contrasts (FXS-TDC) which are associated with significant linear mixed model contrasts.

345 E-F. Brain visualizations depicting least-square means contrasts (t-values) of STP and ERSP of

346 significant interaction effects.

347

Alpha STP increased in FXS females and decreased in FXS males compared to controls.

For alpha STP, a significant group x region x sex interaction effect was present ($F_{13,4973}$=9.6, p <.001). Sex-matched contrasts of alpha STP from the left central region are depicted in **Figures 4C and 4D**. Males with FXS demonstrated decreased alpha STP across the central cortex (LC: t_{71}=-3.2, p=.002, adj. p=.009; RC: t_{71}=-3.3, p=.002, adj. p=.008; **see Table 3**) and increased STP in the left occipital cortex (LO: t_{71}=2.5, p=.015, adj. p=.035). Females with FXS demonstrated a significant (or trending) increase in alpha power across bilateral cortical regions, including central, frontal, cingulate, and parietal regions (t_{71}=2.1-4.3, p=<.001 to .029, adj. p.=<.001 to .07; **see Table 3**).

Table 3. Significant asynchronous single-trial power (STP) contrasts by frequency band.

Variable	Region	Sex	FXS	TDC	DF	F	ES	p	adj. p
STP: Gamma1	LL		-207.3±3.0	-208.7±3.1	71	2.4	.36	.020	.072
	LO		-200.6±4.2	-202.6±4.0	71	3.3	.49	.002	.011
	LT		-199.0±4.0	-201.0±3.7	71	3.9	.45	<.001	.004
	RT		-199.8±4.0	-201.2±3.7	71	2.5	.30	.013	.061
STP: Alpha	LC	F	-193.3±4.9	-196.7±3.7	71	3.6	1.18	<.001	.005
	LC	M	-196.2±2.5	-193.7±2.9	71	-3.2	-.85	.002	.009
	LF	F	-194.7±4.2	-197.8±3.0	71	3.5	1.07	<.001	.005
	LL	F	-195.1±4.1	-199.2±2.8	71	4.5	1.41	<.001	<.001
	LO	M	-193.5±3.2	-195.3±3.7	71	2.5	.64	.015	.035
	LP	F	-196.5±4.5	-199.1±4.4	71	2.9	.90	.006	.019
	LPF	M	-189.9±4.1	-191.4±4.0	71	2.1	.55	.035	.070
	LT	F	-192.5±4.0	-195.2±3.8	71	3.3	.93	.001	.008
	RC	F	-193.3±3.8	-196.1±3.0	71	2.8	.94	.006	.019
	RC	M	-196.0±2.8	-193.4±3.4	71	-3.3	-.88	.002	.008
	RF	F	-195.4±4.2	-197.6±2.9	71	2.5	.76	.015	.035
	RL	F	-195.4±4.0	-199.3±2.7	71	4.3	1.35	<.001	<.001
	RP	F	-196.0±3.4	-198.0±3.5	71	2.2	.70	.029	.064
	RT	F	-193.3±4.3	-195.6±4.0	71	2.8	.79	.007	.019

360 **Table 3.** Significant corrected linear mixed model post-hoc contrasts of least-squared means
361 following correction of STP. Abbreviations: ES, Cohen's *d* effect size; adj. p, 5% false discovery
362 rate corrected p values; FXS, Fragile X Syndrome; TDC, typically developing controls; DF,
363 degrees of freedom; FDR, false discovery rate; LF, left frontal; RF, right frontal; LC, left central;
364 RC, right central; LPF, left prefrontal; LT, left temporal; RT, right temporal; LL, left cingulate; RL,
365 right cingulate; LP, left parietal; RP, right parietal; LO, left occipital.
366
367

Alterations of event related spectral perturbation (ERSP)

Alpha ERSP is decreased in females with FXS

For alpha ERSP, a significant group x sex x region interaction was found ($F_{13,4973}$=2.8, p < .001). Corrected pairwise contrasts demonstrated a significant decrease in alpha ERSP following chirp stimulus in females with FXS in the left temporal and right frontal regions (**see Table 4**). Visualization of t-value region differences between FXS and control females show a broader trend of decreased alpha ERSP across multiple cortical regions (**see Figure 4F**). A significant group x sex x region interaction was found for gamma1 ERSP ($F_{13,4973}$=2.7, p < .001) and gamma2 ERSP ($F_{13,4973}$=2.0, p =.017). No pairwise contrasts survived 5% FDR correction. LME model results for each response variable and any significant interaction effects are summarized in **Supplemental Table 2**. To better visualize gradients and asymmetry in ITPC response across the cortex, we also plotted region contrasts on a three-dimensional glass brain for each measure.

Table 4. Significant event-related spectral perturbation (ERSP) contrasts.

Variable	Region	Sex	FXS	TDC	DF	F	ES	p	adj. p
ERSP: Alpha	LT	F	-.32±.40	-.03±.36	71	-4.2	-.94	<.001	.003
	RF	F	-.22±.40	.03±.36	71	-3.3	-.85	.001	.020
	RT	F	-.26±.32	-.07±.42	71	-2.7	-.61	.009	.088

Table 4. Significant event-related spectral perturbation (ERSP) contrasts. Significant corrected linear mixed model post-hoc contrasts of least-squared means following correction of ERSP. Abbreviations: ES, Cohen's *d* effect size; adj. p, 5% false discovery rate corrected p values; FXS, Fragile X Syndrome; TDC, typically developing controls; DF, degrees of freedom; FDR, false discovery rate; RF, right frontal; LT, left temporal; RT, right temporal.

Increased frontotemporal information flow in males with FXS

We next calculated Renyi transfer entropy (TE) to estimate directional information flow between the right frontal and auditory cortex regions during the onset ITPC response. We hypothesized that greater frontotemporal information flow would be present in FXS. We focused only on the right frontal region as these nodes had significantly greater onset ITPC in FXS (onset ITPC FXS-TDC: caudal middle frontal R (cMFG; t=2.73, p=.001), pars triangularis R (pTRI, t =2.69, p=.011), and rostral middle frontal R (rMFG; t=2.44, p=.019)). We estimated trial-level TE between these three frontal nodes and the right and left superior temporal gyrus (STG; **see Supplementary Figure 3**). Significant connections were determined by bootstrap repetitions [48]. For each subject, we calculated the percentage of trials (out of 60) with significant TE pairs (referred to as TE %) for within sex statistical comparison between groups. We found TE % was increased in males with FXS from the right STG to the right cMFG (t=2.13, p=.04; EF=.63), from the right pTRI to the right STG (t=2.14, p=.04, EF=.63), and the right STG to the right MFG (t=2.96; p=.005, EF=.87) (**see Figure 5A-C**).

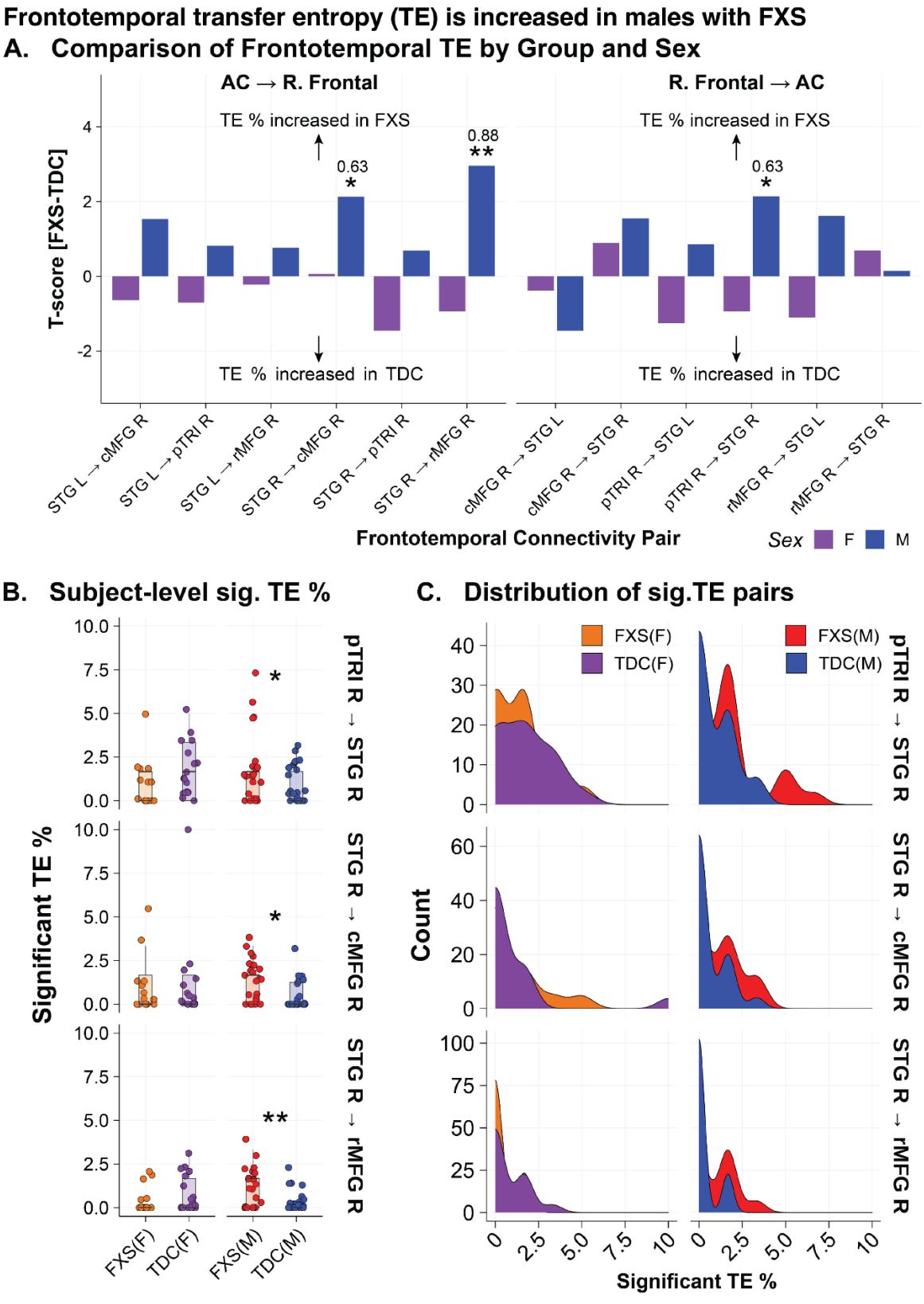

404

405 **Figure 5. Increased frontotemporal information flow in males with Fragile X Syndrome.**

Reyni's transfer entropy (TE) was calculated using source localized time series data between right frontal nodes demonstrating significant (sig.) onset intertrial phase coherence (ITPC) (cMFG, pTRI, rMFG) and the right and left STG (estimated source of the auditory cortex). Bootstrap repetitions were used to determine if a directional connection was significant ($p < .01$). For each subject and node pair, the % of trials demonstrating sig. TE was calculated. A. Group contrasts (within sex) of % of trials demonstrating sig. transfer entropy (TE) by frontotemporal node pairing between FXS and typically developing controls (TDC). Bar plots represent t-score (FXS-TDC) with positive values indicating greater % of trials with sig. TE in the FXS group, while negative values indicate a greater % of trials with sig. TE in the control group. B. Subject-level jitter plot superimposed on boxplots of % of trials with sig. TE across the three sig. frontotemporal pairs. C. Density plot of % of trials with sig. TE across the three sig. frontotemporal pairs. Abbreviations: cMFG, caudal middle frontal; pTRI, pars triangularis; rMFG, rostral middle frontal; STG, superior temporal gyrus; R, right; L, left. Significance: *, $p < .05$; **, $p < .01$. For all boxplots, the center line represents the median, the lower and upper hinges correspond to the 25th and 75th percentiles, and the upper and lower whiskers extend from the hinge to the largest or smallest value, respectively, no further than 1.5 * distance between the 25th and 75th percentiles.

Clinical Correlations

For all FXS participants, we examined 10% FDR corrected Spearman's correlations between bilateral frontal and temporal regions with significant EEG alterations with 13 clinical measures (780 correlations; **see Table 5**). As full mutation males with FXS are expected to have absent or very low levels of FMRP expression, we also explored uncorrected clinical correlations in an FXS male-only subgroup (**see Figure 6A-D and Table 6**).

Measure	Feature	n	rho	p	10% FDR
ADAMS OCD	STP: Left Temporal Gamma1	31	.62	.0002	.0355
ADAMS OCD	STP: Left Temporal Gamma2	31	.64	.0001	.0355
SCQ Total	ITPC: Left Frontal Gamma1	31	-.58	.0007	.0838
SCQ Total	STP: Right Temporal Gamma2	31	.57	.0008	.0838
WJ3	ITPC: Right Frontal Gamma1	28	.71	<.0001	.0167
WJ3	ITPC: Right Temporal Gamma1	28	.64	.0002	.0355
WJ3	ITPC: Right Temporal gamma2	28	.65	.0002	.0355

Table 5. Corrected clinical correlations with EEG features across all FXS participants. Abbreviations: FXS, Fragile X Syndrome; SCQ, Social Communication Questionnaire; WJ-3, Woodcock III Tests of Cognitive Abilities; ADAMS, Anxiety, Depression, and Mood Scale.

Measure	Feature	n	rho	p
ABC FXS: Lethargy/social withdrawal	ITPC: Offset(RT)	20	-.49	.0266
ABC FXS: Hyperactivity/Noncompliance	ITPC: gamma2(LF)	20	-.53	.0174
ABC FXS: Inappropriate speech	ERSP: Gamma2(RT)	20	-.49	.0298
	ITPC: Onset(LF)	20	.49	.0284
	ITPC: Onset(RF)	20	.55	.0128
	ITPC: Onset(RT)	20	.47	.0368
ADAMS General Anxiety	ERSP: Gamma1(LO)	21	.45	.0421
	ITPC: Onset(RT)	21	.50	.0224
ADAMS Obsessive/Compliance Behavior	ERSP: Gamma1(RF)	21	-.46	.0367
	ITPC: Offset(RT)	21	-.51	.0173
Age at Visit	ERSP: Alpha(LF)	23	-.48	.0198
	ITPC: Gamma1(RO)	23	.46	.0263
	ITPC: Gamma1(RT)	23	.43	.0412
Deviation IQ	ITPC: Gamma1(LT)	22	.44	.0423
NVIQ Z Score	ITPC: Gamma1(LT)	22	.48	.0244
VIQ Z Score	ITPC: Gamma1(LF)	22	.45	.0348
	ITPC: Gamma2(LF)	22	.62	.0021
WJ3	ERSP: Gamma2(LT)	20	.50	.0253
	ERSP: Gamma2(RO)	20	-.47	.0373
	ITPC: Gamma1(LO)	20	.52	.0193
	ITPC: Gamma1(LT)	20	.52	.0175
	ITPC: Gamma1(RF)	20	.72	.0003
	ITPC: Gamma1(RO)	20	.55	.0118
	ITPC: Gamma1(RT)	20	.65	.0017
	ITPC: Gamma2(RT)	20	.60	.0054

Table 6. Uncorrected clinical correlations with chirp EEG features across the subgroup of males with FXS. Abbreviations: FXS, Fragile X Syndrome; NVIQ, Non-verbal intelligence scale; VIQ, verbal intelligence scale; SCQ, Social Communication Questionnaire; ABC, Aberrant Behavior Checklist; WJ-3, Woodcock III Tests of Cognitive Abilities; ADAMS, Anxiety, Depression, and Mood Scale.

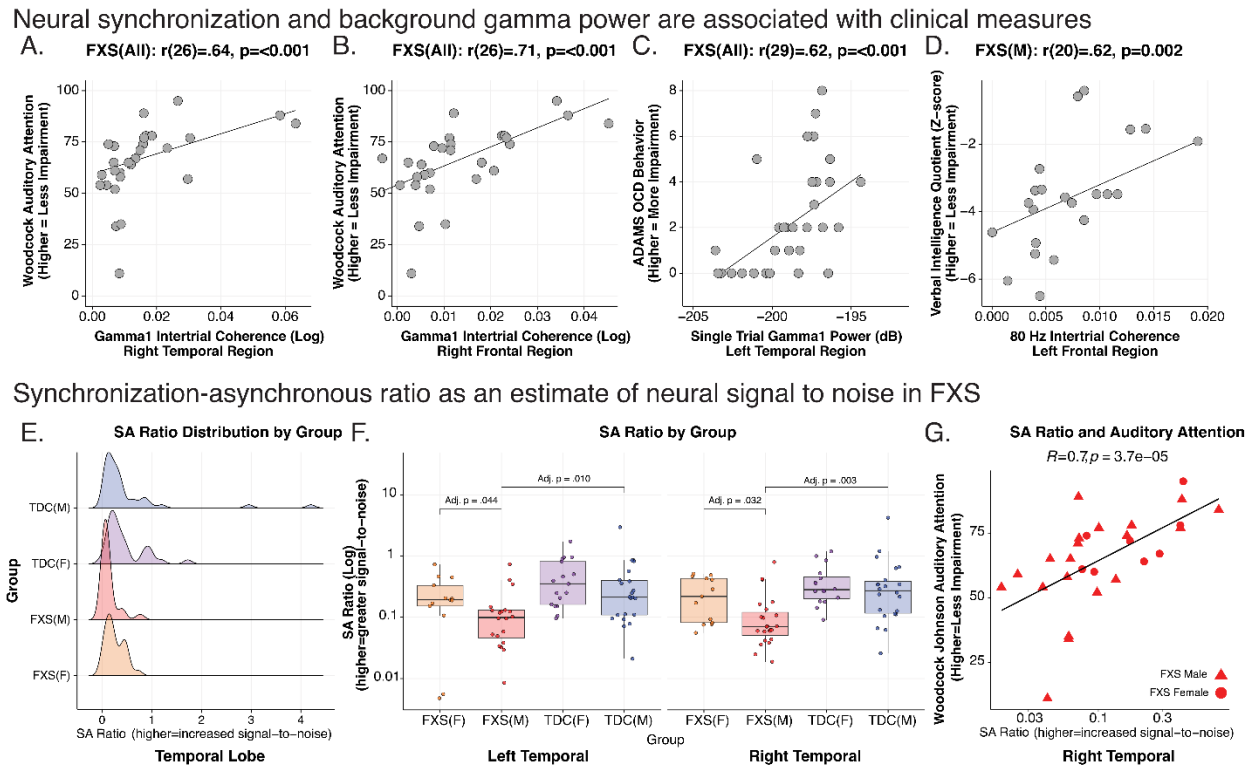

Figure 6. Clinical Correlations and Neurobehavioral Biomarker. Neural synchronization and background gamma power are associated with clinical measures. A-D. Exemplar scatter plots of clinical correlations with EEG variables across all Fragile X Syndrome (FXS) subjects, and a subgroup of full mutation males are shown. Scatterplots in each box depict subject-level bivariate Spearman's correlations. E-G. Synchronization-asynchronization ratio (SA ratio) estimates neural signal to noise (SNR) in FXS. The SA ratio is a composite measure of the degree of gamma1 neural synchronization ("phase locking") as a ratio of background gamma power ("noise"). E. Distribution of SA in males with FXS is skewed towards a lower SA ratio (reduced SNR). F. Boxplots with superimposed scatter plot of SA ratio: Data points represent the average SA ratio within the right and left temporal region per subject. SA ratio in males with FXS is significantly reduced in bilateral temporal regions compared to either control males or females with FXS (see Table 7). For all boxplots, the center line represents the median, the lower and upper hinges correspond to the 25th and 75th percentiles), and the upper and lower whiskers extend from the hinge to the largest or smallest value, respectively, no further than 1.5 times the distance between

457 the 25th and 75th percentiles. G. Temporal SA ratio is highly correlated with auditory attention, so

458 greater SNR is associated with better auditory attention performance.

459

Auditory Attention.

All FXS: The WJ3 quantifies selective auditory attention (including speech-sound discrimination and resistance to auditory stimulus distraction), with higher scores indicating better performance[36]. The task can be reliably performed in children and those with intellectual disability. We found a positive correlation between WJ3 auditory attention task performance and phase locking with Gamma1 ITPC (right temporal: rho(27)=.64; p<.001, adj. p=.035; see Figure 6A; right frontal: rho(27)=.71; p<.001, adj. p=.017; see Figure 6B) and gamma2 ITPC (right temporal: rho(27)=.65; p<.001, adj. p=.035). FXS Males: This association of gamma1 ITPC and WJ3 was preserved in the subgroup of males with FXS (**see Table 6**).

Other clinical measures.

All FXS: Higher (worse) Anxiety, Depression, and Mood Scale (ADAMS) obsessive severity scores were associated with increased left temporal gamma1 (left temporal: rho(30)=.62; p<.001, 5% FDR p=.035; see Figure 6C) and gamma2 STP (left temporal: rho(30)=.64; p<.001, 5% FDR p=.035). We found trend level associations (10% FDR) such that decreased gamma1 ITPC (left frontal: rho(30)=-.58; p<.001, 5% FDR p=.083) and increased gamma2 STP (right temporal: rho(30)=.64; p<.001, 5% FDR p=.083) were associated with SCQ (social communication impairment). In FXS males (see Table 6), higher left temporal gamma1 ITPC was associated with higher non-verbal and full-scale IQ scores. Increased left frontal gamma1 and gamma2 ITPC was correlated with increased verbal IQ (**see Figure 6D**). Onset ITPC of bilateral frontal and right temporal regions were associated with ABC measures of inappropriate speech. Higher levels of gamma1 and gamma2 ERSP were associated with worsening ADAMS anxiety scores, OCD scale scores and ABC inappropriate speech. ERSP alpha power was inversely related to age at visit.

Transfer Entropy

Uncorrected Spearman correlation of TE % and cognitive measures within males with FXS revealed a moderate, negative correlation between TE % of the pTRI R to the STG R and

intelligence (FSIQ: r = -0.610, p = 0.003, n = 22) and verbal z-score (r = -0.497, p = 0.02, n = 22). This negative correlation suggests that higher frontotemporal information flow in these specific brain regions may be associated with lower cognitive performance in males with FXS.

Gamma synchronous-asynchronous (SA) ratio suggests reduced signal-to-noise ratio of auditory processing in FXS.

Individuals with FXS had increased background gamma1 STP, though the gamma1 ITPC deficit was primarily present in males. We hypothesized that the relationship between gamma phase synchrony (gamma ITPC) and background elevation in unsynchronized gamma power (STP) would be an indicator of signal-to-noise ratio (SNR), with lower signal-to-noise ratio being associated with hyperacusis[56]. We calculated the ratio of gamma1 ITPC and gamma1 STP to derive a synchronous-to-asynchronous ratio (SA ratio). Gamma1 STP values were normalized between 0 and the maximum of gamma1 ITPC (.0164) to ensure similar scales between measures. A higher SA ratio indicates more stimulus phase locking ("signal") relative to background gamma power ("noise") (see Eq. 4).

Eq. 4 $$synchronous - to - asynchronous_{ratio} = \frac{gamma1\ ITPC}{gamma1\ STP}$$

We focused on the SA ratio within the temporal lobes where ITPC and STP impairment was detected and the location of AC. We calculated the average SA ratio within the left and right temporal lobes for each subject (**see Figure 6E**). A Wilcoxon Signed-Ranks Test indicated that the SA ratio was diminished in males with FXS compared to females with FXS and control participants (**see Figure 6F and Table 7**). Highlighting the functional importance of this SNR index, we observed a significant positive correlation between the SA ratio in auditory cortex and WJ3 auditory attention task performance across FXS participants (R=.70, p=3.7e-5; **see Figure 6G and Table 7**).

Region	Side	*g1*	*g2*	*(g1-g2)*	95% CI	W	ES	p	Adj. p
Temporal	Left	FXS(M)	TDC(F)	-1.66	[-3.26 -.81]	43	.61	7.4e-06	4.4e-05
		FXS(M)	TDC(M)	-.89	[-1.83 -.42]	118	.49	2.0e-03	9.0e-03
		FXS(M)	FXS(F)	-.80	[.28 1.41]	227	.42	0.01	0.039
		FXS(F)	TDC(F)	-1.04	[-2.92 .18]	70	.25	0.094	0.284
		FXS(F)	TDC(M)	-.26	[-1.44 .66]	121	.11	0.468	0.468
		TDC(F)	TDC(M)	.62	[-.36 2.16]	236	.16	0.172	0.344
	Right	FXS(M)	TDC(F)	-1.45	[-2.19 -.79]	66	.61	2.2e-04	1.0e-03
		FXS(M)	TDC(M)	-1.24	[-1.96 -.37]	105	.49	5.4e-04	3.0e-03
		FXS(M)	FXS(F)	-.75	[.12 2.31]	232	.42	6.0e-03	0.023
		FXS(F)	TDC(F)	-.61	[-1.68 .80]	88	.25	0.363	1
		FXS(F)	TDC(M)	-.25	[-1.53 .84]	127	.11	0.601	1
		TDC(F)	TDC(M)	.25	[-.91 1.24]	206	.16	0.604	1

Table 7: The synchronous-to-asynchronous (SA) ratio was developed as a proposed signal-to-noise biomarker to estimate the efficiency of auditory processing in FXS. Abbreviations: g1, Group 1; g2, Group 2; FXS, Fragile X Syndrome; TDC, Typically Developing Controls; CI, confidence interval; W, Wilcoxon Statistic, ES, Wilcoxon effect size; Adj. p, Bonferroni-Holm corrected adjusted p values.

Discussion

The mechanisms underlying auditory hypersensitivity in FXS have not yet been established. Understanding these mechanisms has broad implications as sensory alterations are impairing and highly prevalent across neurodevelopmental disorders[57–60]. Using a well-powered case-control study, we examined the spatiotemporal characteristics of neural response to the chirp stimulus. Our objective was to characterize the spatiotemporal characteristics of gamma abnormalities associated with auditory processing of the chirp stimulus in FXS. Our major findings in FXS include 1) a marked increase in onset phase synchronization in frontal regions, 2) reduced chirp synchronization and increased background activity in temporal regions, 3) increased frontotemporal information exchange, 4) mediation by sex for these key alterations, and 5) robust associations between clinical measures and EEG changes. These systems-level alterations may serve as biomarkers of target engagement for treatments aimed at reducing hyperarousal and improving regulation of sensory systems. The results create opportunities for back-translation by testing circuit-level mechanisms of the observed functional changes in *Fmr1*$^{-/-}$ knockout mouse models [54,61].

Frontal Region Hyperresponsiveness and Frontotemporal Connectivity

The frontal regions of individuals with FXS showed a heightened onset ITPC response (157-165% vs. controls) to the chirp stimulus. In males with FXS, this increase in onset ITPC was associated with worsening anxiety scores. While it is typical for frontal and temporal regions to reciprocate activity in normative populations during early auditory processing [62–64], our results suggest that individuals with FXS have exaggerated salience or orientation to sensory stimulation in FXS, which could contribute to heightened anxiety levels. These functional changes may be related to alterations in frontal structure and maturation as observed from neuroimaging studies on FXS [3,4,65–68]. Through effective connectivity analysis, we discovered an increase in

reciprocal information flow between frontotemporal regions. The auditory pathway from the brainstem to the cortex is particularly rich in FMRP-expressing neurons [69], and the loss of FMRP is known to alter the functional and structural properties of the auditory system [70,71]. The increase in information flow was negatively correlated with cognitive function. These findings suggest that there may be a breakdown in the top-down regulatory processes responsible for filtering out irrelevant sensory information in FXS. Consequently, individuals with FXS might have an over-responsiveness of the auditory cortex to incoming auditory stimuli contributing to hyperacusis and anxiety observed [24,25]. The observed variation in frontal input may also explain the heterogeneity in auditory sensitivity observed clinically in FXS - some individuals with FXS display distress to certain noises while others may enjoy loud music [57]. These alterations in frontotemporal connectivity suggest that the integration of bottom-up sensory and top-down frontal processes influences whether sounds are perceived as pleasurable or aversive in context.

Localization of gamma synchronization and background power alterations in FXS

Control subjects typically demonstrate strong phase synchronization to the auditory chirp stimulus in the gamma frequency band (~40 Hz), which allows for effective encoding and selective enhancement of the stimulus over background noise [7]. In individuals with FXS, we significant impairments in gamma phase alignment and an increase in asynchronous background gamma power in the temporal lobe regions. These findings were strongly associated with obsessive behavior, as well as alterations in social communication and auditory attention. In males with FXS, deficits in gamma synchronization in frontal regions were linked to greater reductions in verbal intelligence, auditory attention, and hyperactivity/impulsivity. By similar findings with trend-level significance after correction for multiple comparisons (e.g., effects significant at 10% but not 5% FDR), a more comprehensive understanding of abnormalities in the FXS functional auditory

system emerges. Alterations in synchronization in FXS appear to occur in both bilateral temporal and prefrontal cortex, right parietal cortex, and cingulate sources, all of which play roles in auditory processing[64,72–74]. This suggests dysfunction in filtering irrelevant auditory information and maintaining an optimal excitatory-inhibitory balance. Interestingly, though excitatory-inhibitory balance may be altered, we speculate that the auditory system may otherwise have reached an "imperfect homeostasis" with basic hearing functions maintained, but struggling to cope with more complex demands and lacking the ability to compensate, leading to hypersensitivity and startle responses[60,75].

Event-related gamma activity in FXS is elevated and stimulus-independent

How do we best reconcile 1) reduced gamma synchronization, 2) increased gamma background power, and 3) no change in gamma stimulus evoked power in FXS during the chirp? Though we previously reported these findings in scalp recordings of the chirp response, we have now effectively disentangled temporal and frontal contributions to these alterations. The temporal lobe findings are reminiscent of *Fmr1*$^{-/-}$ KO brain slice microcircuits experiments in which gamma oscillations exhibit hyper-synchrony that is stimulus independent and not responsive to phase reset[21]. For example, disordered and incongruent firing patterns are observed in extracellular recordings from layer 4 of the *Fmr1*$^{-/-}$ KO somatosensory cortex[76,77] and auditory cortex[21]. The SA ratio captured the relationship between neural synchronization and background asynchronous activity of gamma activity within the temporal regions. We speculate that in FXS, engagement of cortical circuitry via the input sound leads to increased activity (i.e., gamma STP) but does not lead to the expected phase reset of gamma oscillations in relation to the frequency of sensory input (e.g., gamma1 ITPC). We found significantly lower SA ratios in males with FXS. Across all FXS subjects, the high degree of association between increased SA ratios and increased auditory attention performance highlights the clinical significance of our findings.

Observed sex differences may reveal compensatory action of alpha

Our findings reveal inherent inefficiencies in temporal lobe auditory processing in Fragile X Syndrome (FXS), with sex differences. In males, reduced gamma phase synchronization and elevated asynchronous gamma power in temporal regions may indicate impairments associated with basic sensory function [78,79]. In contrast, females with FXS showed intact temporal synchronization and gamma power, along with higher signal-to-noise ratio performance, suggesting relatively spared auditory processing. While auditory hypersensitivity is common in FXS [57], the degree of sensory distress differs from person to person and is not universal and may be explained by variations in the distribution and level of FMRP expression in the auditory system) [69]. Interestingly, we observed markedly increased alpha power in females with FXS localized to deeper brain structures (cingulate or other regions such as the inferior colliculus) [80]. It is well-established that alpha power is significantly reduced in males with FXS [15,16,81–83] and proposed to represent thalamocortical dysfunction [16,84]. When considered in the context of alpha canonical role in functional inhibition, it may be that intact alpha generation in females may mitigate hyperexcitability impairments by gating information flow[85–87, 91]. For example, when a stimulus is presented against background noise in controls, alpha power is increased in occipital and temporal regions[86,88]. Elucidating potential protective factors in females, including enhancement of alpha oscillations, could inform the development of novel therapies targeting sensory hypersensitivity across both sexes in FXS.

Limitations

Certain limitations of the current study should be taken into when interpreting the results. First, the study only included FXS and control groups. It would be advantageous to include control groups with consist of individuals who are IQ matched with other neurodevelopmental conditions

617 to determine the specificity of our observations to FXS. Second, increasing the number of females
618 and targeting specific age groups would enhance understanding of sex and developmental
619 effects. Third, as excluding medicated patients would disproportionately reduce the
620 representation of individuals with more severe clinical presentations, we opted to include such
621 cases. While we reported no differences in chirp response between medicated and non-
622 medicated patients [14], current medication treatments might impact the reported findings. We
623 excluded individuals receiving antiepileptic medications, which are known to affect EEG
624 measures. In addition to these clinical considerations, the current findings are specific to the
625 auditory system, and it is uncertain if the findings will apply to other modalities. Due to a lack of
626 individual anatomical data, we utilized a standardized anatomical atlas (ICBM152) to compute the
627 electric lead field for the EEG source modeling. While individual MRI scans can improve accuracy,
628 prior studies have shown that EEG source estimates have sufficient spatial resolution to justify
629 forgoing individual anatomy in certain contexts [40,89]. In addition, we examined cortical regions
630 and used atlas nodes as replicates, taking a conservative approach with regards to the spatial
631 precision of our analysis. There remain practical challenges with quantifying sensory
632 hypersensitivity in individuals with intellectual disability by self- or caregiver report [90]. Instead,
633 we used an alternative strategy by using an auditory attention task that includes both top-down
634 cognitive processing and sensory perception that offers a more objective and feasible means of
635 assessment applicable to participants of varying functional levels [36].
636

637 ## Conclusion

638 Our study demonstrates distinct spatial and behavioral correlates of abnormal auditory
639 processing in FXS. The functional auditory system in FXS displays differences by region and has
640 altered heuristics in detecting signal to noise. Males with FXS display excessive frontal activation
641 upon hearing a stimulus, which suggests a disruption in the modulatory influence of top-down

642 pathway from the frontal to the auditory cortex in influencing auditory processing. Across males
643 and females with FXS, asynchronous gamma activity is elevated and rigid, which may constrain
644 the function of the auditory system. The findings of this study are significant for back translation,
645 as they offer more precise electrophysiological phenotypes to target in future research utilizing
646 region-selective or cell-selective conditional knock-out. They also have implications for
647 therapeutic targets in locally rigid circuits and are relevant for signal-to-noise conceptual
648 frameworks in understanding apparent paradoxical neural activity in neurodevelopmental
649 disorders.
650

651 # Acknowledgements

652 Dr. Sweeney passed away before the submission of the final version of this manuscript, Dr.
653 Pedapati accepts responsibility for the integrity and validity of the data collected and analyzed.
654 Dr. Sweeney played an integral role in the conception and development of the ideas presented.
655

References

1. Hagerman RJ, Berry-Kravis E, Hazlett HC, Bailey DB, Moine H, Kooy RF, et al. Fragile X syndrome. Nature reviews Disease primers. 2017;3: 17065.
2. Salvi R, Chen G-D, Manohar S. Hyperacusis: Loudness intolerance, fear, annoyance and pain. Hear Res. 2022;426: 108648.
3. Rivera SM, Menon V, White CD, Glaser B, Reiss AL. Functional brain activation during arithmetic processing in females with fragile X Syndrome is related to FMR1 protein expression. Hum Brain Mapp. 2002;16: 206–218.
4. Hoeft F, Hernandez A, Parthasarathy S, Watson CL, Hall SS, Reiss AL. Fronto-striatal dysfunction and potential compensatory mechanisms in male adolescents with fragile X syndrome. Hum Brain Mapp. 2007;28: 543–554.
5. Barnea-Goraly N, Eliez S, Hedeus M, Menon V, White CD, Moseley M, et al. White matter tract alterations in fragile X syndrome: preliminary evidence from diffusion tensor imaging. Am J Med Genet B Neuropsychiatr Genet. 2003;118B: 81–88.
6. Lee CC. Thalamic and cortical pathways supporting auditory processing. Brain Lang. 2013;126: 22–28.
7. Artieda J, Valencia M, Alegre M, Olaziregi O, Urrestarazu E, Iriarte J. Potentials evoked by chirp-modulated tones: a new technique to evaluate oscillatory activity in the auditory pathway. Clin Neurophysiol. 2004;115: 699–709.
8. Fries P. Rhythms for Cognition: Communication through Coherence. Neuron. 2015;88: 220–235.
9. Fries P. A mechanism for cognitive dynamics: neuronal communication through neuronal coherence. Trends Cogn Sci. 2005;9: 474–480.
10. Paik S-B, Glaser DA. Synaptic Plasticity Controls Sensory Responses through Frequency-Dependent Gamma Oscillation Resonance. PLoS Comput Biol. 2010;6.

11. Orekhova EV, Stroganova TA, Schneiderman JF, Lundstrˆm S, Riaz B, Sarovic D, et al. Neural gain control measured through cortical gamma oscillations is associated with sensory sensitivity. Hum Brain Mapp. 2019;40: 1583–1593.
12. Ethridge LE, White SP, Mosconi MW, Wang J, Byerly MJ, Sweeney JA. Reduced habituation of auditory evoked potentials indicate cortical hyper-excitability in Fragile X Syndrome. Transl Psychiatry. 2016;6: e787.
13. Ethridge LE, White SP, Mosconi MW, Wang J, Pedapati EV, Erickson CA, et al. Neural synchronization deficits linked to cortical hyper-excitability and auditory hypersensitivity in fragile X syndrome. Mol Autism. 2017;8: 22.
14. Ethridge LE, De Stefano LA, Schmitt LM, Woodruff NE, Brown KL, Tran M, et al. Auditory EEG Biomarkers in Fragile X Syndrome: Clinical Relevance. Front Integr Neurosci. 2019;13: 60.
15. Wang J, Ethridge LE, Mosconi MW, White SP, Binder DK, Pedapati EV, et al. A resting EEG study of neocortical hyperexcitability and altered functional connectivity in fragile X syndrome. J Neurodev Disord. 2017;9: 11.
16. Pedapati EV, Schmitt LM, Ethridge LE, Miyakoshi M, Sweeney JA, Liu R, et al. Neocortical localization and thalamocortical modulation of neuronal hyperexcitability contribute to Fragile X Syndrome. Commun Biol. 2022;5: 442.
17. Schmitt LM, Li J, Liu R, Horn PS, Sweeney JA, Erickson CA, et al. Altered frontal connectivity as a mechanism for executive function deficits in fragile X syndrome. Mol Autism. 2022;13: 47.
18. Wilkinson CL, Nelson CA. Increased aperiodic gamma power in young boys with Fragile X Syndrome is associated with better language ability. Mol Autism. 2021;12: 17.
19. Schmitt LM, Wang J, Pedapati EV, Thurman AJ, Abbeduto L, Erickson CA, et al. A neurophysiological model of speech production deficits in fragile X syndrome. Brain Commun. 2020;2: fcz042.

20. Jonak CR, Lovelace JW, Ethell IM, Razak KA, Binder DK. Multielectrode array analysis of EEG biomarkers in a mouse model of Fragile X Syndrome. Neurobiol Dis. 2020;138: 104794.
21. Goswami S, Cavalier S, Sridhar V, Huber KM, Gibson JR. Local cortical circuit correlates of altered EEG in the mouse model of Fragile X syndrome. Neurobiol Dis. 2019;124: 563–572.
22. Antar LN, Bassell GJ. Sunrise at the synapse: the FMRP mRNP shaping the synaptic interface. Neuron. 2003;37: 555–558.
23. Richter JD, Zhao X. The molecular biology of FMRP: new insights into fragile X syndrome. Nat Rev Neurosci. 2021;22: 209–222.
24. Gomot M, Giard M-H, Adrien J-L, Barthelemy C, Bruneau N. Hypersensitivity to acoustic change in children with autism: Electrophysiological evidence of left frontal cortex dysfunctioning. Psychophysiology. 2002;39: 577–584.
25. Gomes E, Rotta NT, Pedroso FS, Sleifer P, Danesi MC. Auditory hypersensitivity in children and teenagers with autistic spectrum disorder. Arq Neuropsiquiatr. 2004;62: 797–801.
26. Lucker JR. Auditory Hypersensitivity in Children With Autism Spectrum Disorders: http://dx.doi.org.uc.idm.oclc.org/101177/1088357613475810. 2013. doi:10.1177_1088357613475810
27. Todorovic A, van Ede F, Maris E, de Lange FP. Prior expectation mediates neural adaptation to repeated sounds in the auditory cortex: an MEG study. J Neurosci. 2011;31: 9118–9123.
28. Winkowski DE, Nagode DA, Donaldson KJ, Yin P, Shamma SA, Fritz JB, et al. Orbitofrontal Cortex Neurons Respond to Sound and Activate Primary Auditory Cortex Neurons. Cereb Cortex. 2018;28: 868–879.
29. Inui K, Okamoto H, Miki K, Gunji A, Kakigi R. Serial and parallel processing in the human auditory cortex: a magnetoencephalographic study. Cereb Cortex. 2006;16: 18–30.

30. Song J, Davey C, Poulsen C, Luu P, Turovets S, Anderson E, et al. EEG source localization: Sensor density and head surface coverage. J Neurosci Methods. 2015;256: 9–21.
31. Coffey EBJ, Nicol T, White-Schwoch T, Chandrasekaran B, Krizman J, Skoe E, et al. Evolving perspectives on the sources of the frequency-following response. Nat Commun. 2019;10: 5036.
32. Yamasaki H, LaBar KS, McCarthy G. Dissociable prefrontal brain systems for attention and emotion. Proc Natl Acad Sci U S A. 2002;99: 11447–11451.
33. Boggs AE, Schmitt LM, McLane RD, Adayev T, LaFauci G, Horn PS, et al. Optimization, validation and initial clinical implications of a Luminex-based immunoassay for the quantification of Fragile X Protein from dried blood spots. Sci Rep. 2022;12: 5617.
34. Valdovinos MG, Parsa RA, Alexander ML. Results of a nation-wide survey evaluating psychotropic medication use in fragile X syndrome. J Dev Phys Disabil. 2009;21: 23–37.
35. Sansone SM, Schneider A, Bickel E, Berry-Kravis E, Prescott C, Hessl D. Improving IQ measurement in intellectual disabilities using true deviation from population norms. J Neurodev Disord. 2014;6: 16.
36. McGrew KS, Woodcock RW. Woodcock-Johnson III Technical Manual: WJ III. Riverside Publ.; 2006.
37. Esbensen AJ, Rojahn J, Aman MG, Ruedrich S. Reliability and validity of an assessment instrument for anxiety, depression, and mood among individuals with mental retardation. J Autism Dev Disord. 2003;33: 617–629.
38. Sansone SM, Widaman KF, Hall SS, Reiss AL, Lightbody A, Kaufmann WE, et al. Psychometric study of the Aberrant Behavior Checklist in Fragile X Syndrome and implications for targeted treatment. J Autism Dev Disord. 2012;42: 1377–1392.
39. Delorme A, Makeig S. EEGLAB: an open source toolbox for analysis of single-trial EEG dynamics including independent component analysis. J Neurosci Methods. 2004;134: 9–21.

759 40. Tadel F, Baillet S, Mosher JC, Pantazis D, Leahy RM. Brainstorm: a user-friendly
760 application for MEG/EEG analysis. Comput Intell Neurosci. 2011;2011: 879716.
761 41. Grech R, Cassar T, Muscat J, Camilleri KP, Fabri SG, Zervakis M, et al. Review on solving
762 the inverse problem in EEG source analysis. J Neuroeng Rehabil. 2008;5: 25.
763 42. Hincapié A-S, Kujala J, Mattout J, Daligault S, Delpuech C, Mery D, et al. MEG
764 Connectivity and Power Detections with Minimum Norm Estimates Require Different
765 Regularization Parameters. Comput Intell Neurosci. 2016;2016: 3979547.
766 43. Lin F-H, Witzel T, Ahlfors SP, Stufflebeam SM, Belliveau JW, Hämäläinen MS. Assessing
767 and improving the spatial accuracy in MEG source localization by depth-weighted
768 minimum-norm estimates. Neuroimage. 2006;31: 160–171.
769 44. Mazziotta JC, Toga AW, Evans A, Fox P, Lancaster J. A probabilistic atlas of the human
770 brain: Theory and rationale for its development. Neuroimage. 1995;2: 89–101.
771 45. Gramfort A, Papadopoulo T, Olivi E, Clerc M. OpenMEEG: opensource software for
772 quasistatic bioelectromagnetics. Biomed Eng Online. 2010;9: 45.
773 46. Desikan RS, Segonne F, Fischl B, Quinn BT, Dickerson BC, Blacker D, et al. An automated
774 labeling system for subdividing the human cerebral cortex on MRI scans into gyral based
775 regions of interest. Neuroimage. 2006;31: 968–980.
776 47. Wibral M, Vicente R, Lindner M. Transfer Entropy in Neuroscience. In: Wibral M, Vicente R,
777 Lizier JT, editors. Directed Information Measures in Neuroscience. Berlin, Heidelberg:
778 Springer Berlin Heidelberg; 2014. pp. 3–36.
779 48. Behrendt S, Zimmermann D, Dimpfl T, Peter F. RTransferEntropy: Measuring Information
780 Flow Between Time Series with Shannon and Renyi Transfer Entropy. R package version
781 0.2; 2019.
782 49. De La Pava Panche I, Alvarez-Meza AM, Orozco-Gutierrez A. A Data-Driven Measure of
783 Effective Connectivity Based on Renyi's α-Entropy. Front Neurosci. 2019;13: 1277.
784 50. Dimpfl T, Peter FJ. Using transfer entropy to measure information flows between financial

markets. Stud Nonlinear Dyn Econom. 2013;17: 85–102.

51. Pinheiro J, Bates D. Mixed-effects models in S and S-PLUS. Springer science & business media; 2006.

52. Benjamini Y, Hochberg Y. Controlling the false discovery rate: a practical and powerful approach to multiple testing. J R Stat Soc Series B Stat Methodol. 1995; 289–300.

53. Seeber M, Cantonas LM, Hoevels M, Sesia T, Visser-Vandewalle V, Michel CM. Subcortical electrophysiological activity is detectable with high-density EEG source imaging. Nat Commun. 2019;10: 753.

54. Lovelace JW, Rais M, Palacios AR, Shuai XS, Bishay S, Popa O, et al. Deletion of Fmr1 from Forebrain Excitatory Neurons Triggers Abnormal Cellular, EEG, and Behavioral Phenotypes in the Auditory Cortex of a Mouse Model of Fragile X Syndrome. Cereb Cortex. 2020;30: 969–988.

55. Sinclair D, Featherstone R, Naschek M, Nam J, Du A, Wright S, et al. GABA-B Agonist Baclofen Normalizes Auditory-Evoked Neural Oscillations and Behavioral Deficits in the Fmr1 Knockout Mouse Model of Fragile X Syndrome. eNeuro. 2017;4. doi:10.1523/ENEURO.0380-16.2017

56. Crone NE, Boatman D, Gordon B, Hao L. Induced electrocorticographic gamma activity during auditory perception. Clin Neurophysiol. 2001;112: 565–582.

57. Rais M, Binder DK, Razak KA, Ethell IM. Sensory Processing Phenotypes in Fragile X Syndrome. ASN Neuro. 2018;10: 1759091418801092.

58. Sinclair D, Oranje B, Razak KA, Siegel SJ, Schmid S. Sensory processing in autism spectrum disorders and Fragile X syndrome—From the clinic to animal models. Neurosci Biobehav Rev. 2017;76: 235–253.

59. Rotschafer S, Razak K. Auditory Processing in Fragile X Syndrome. Front Cell Neurosci. 2014;8. doi:10.3389/fncel.2014.00019

60. Liu X, Kumar V, Tsai N-P, Auerbach BD. Hyperexcitability and Homeostasis in Fragile X

811 Syndrome. Front Mol Neurosci. 2021;14: 805929.
812 61. Rotschafer S, Razak K. Altered auditory processing in a mouse model of fragile X
813 syndrome. Brain Res. 2013;1506: 12–24.
814 62. Newman JD, Lindsley DF. Single unit analysis of auditory processing in squirrel monkey
815 frontal cortex. Exp Brain Res. 1976;25: 169–181.
816 63. Alegre M, Barbosa C, Valencia M, Pérez-Alcázar M, Iriarte J, Artieda J. Effect of Reduced
817 Attention on Auditory Amplitude-Modulation Following Responses: A Study With Chirp-
818 Evoked Potentials. J Clin Neurophysiol. 2008;25. Available:
819 https://journals.lww.com/clinicalneurophys/Fulltext/2008/02000/Effect_of_Reduced_Attentio
820 n_on_Auditory.6.aspx
821 64. Plakke B, Romanski LM. Auditory connections and functions of prefrontal cortex. Front
822 Neurosci. 2014;8: 199.
823 65. Mazzocco MMM, Hagerman RJ, Cronister-Silverman A, Pennington BF. Specific frontal
824 lobe deficits among women with the fragile X gene. J Am Acad Child Adolesc Psychiatry.
825 1992;31: 1141–1148.
826 66. Menon V, Leroux J, White CD, Reiss AL. Frontostriatal deficits in fragile X syndrome:
827 relation to FMR1 gene expression. Proc Natl Acad Sci U S A. 2004;101: 3615–3620.
828 67. Haas BW, Barnea-Goraly N, Lightbody AA, Patnaik SS, Hoeft F, Hazlett H, et al. Early
829 white-matter abnormalities of the ventral frontostriatal pathway in fragile X syndrome. Dev
830 Med Child Neurol. 2009;51: 593–599.
831 68. Bray S, Hirt M, Jo B, Hall SS, Lightbody AA, Walter E, et al. Aberrant frontal lobe
832 maturation in adolescents with fragile X syndrome is related to delayed cognitive
833 maturation. Biol Psychiatry. 2011;70: 852–858.
834 69. Zorio DAR, Jackson CM, Liu Y, Rubel EW, Wang Y. Cellular distribution of the fragile X
835 mental retardation protein in the mouse brain. J Comp Neurol. 2017;525: 818–849.
836 70. McCullagh EA, Rotschafer SE, Auerbach BD, Klug A, Kaczmarek LK, Cramer KS, et al.

Mechanisms underlying auditory processing deficits in Fragile X syndrome. The FASEB Journal. 2020;34: 3501–3518.

71. Wang X, Kohl A, Yu X, Zorio DAR, Klar A, Sela-Donenfeld D, et al. Temporal-specific roles of fragile X mental retardation protein in the development of the hindbrain auditory circuit. Development. 2020;147. doi:10.1242/dev.188797

72. Oya H, Gander PE, Petkov CI, Adolphs R, Nourski KV, Kawasaki H, et al. Neural phase locking predicts BOLD response in human auditory cortex. Neuroimage. 2018;169: 286–301.

73. Griffiths TD. Spatial and temporal auditory processing deficits following right hemisphere infarction: a psychophysical study. Neurocase. 1998;5: 69b–679.

74. Karhson DS, Mock JR, Golob EJ. The role of right inferior parietal cortex in auditory spatial attention: A repetitive transcranial magnetic stimulation study. PLoS One. 2015;10: e0144221.

75. Antoine MW, Langberg T, Schnepel P, Feldman DE. Increased Excitation-Inhibition Ratio Stabilizes Synapse and Circuit Excitability in Four Autism Mouse Models. Neuron. 2019;101: 648-661 e4.

76. Gibson JR, Bartley AF, Hays SA, Huber KM. Imbalance of neocortical excitation and inhibition and altered UP states reflect network hyperexcitability in the mouse model of fragile X syndrome. J Neurophysiol. 2008;100: 2615–2626.

77. Hays SA, Huber KM, Gibson JR. Altered neocortical rhythmic activity states in Fmr1 KO mice are due to enhanced mGluR5 signaling and involve changes in excitatory circuitry. Journal of Neuroscience. 2011;31: 14223–14234.

78. Hullett PW, Hamilton LS, Mesgarani N, Schreiner CE, Chang EF. Human superior temporal gyrus organization of spectrotemporal modulation tuning derived from speech stimuli. J Neurosci. 2016;36: 2014–2026.

79. So NLT, Edwards JA, Woolley SMN. Auditory selectivity for spectral contrast in cortical

neurons and behavior. J Neurosci. 2020;40: 1015–1027.

80. Billig AJ, Lad M, Sedley W, Griffiths TD. The hearing hippocampus. Prog Neurobiol. 2022;218: 102326.

81. Van der Molen MJ, Van der Molen MW. Reduced alpha and exaggerated theta power during the resting-state EEG in fragile X syndrome. Biol Psychol. 2013;92: 216–219.

82. van der Molen MJ, Stam CJ, van der Molen MW. Resting-state EEG oscillatory dynamics in fragile X syndrome: abnormal functional connectivity and brain network organization. PLoS One. 2014;9: e88451.

83. Smith EG, Pedapati EV, Liu R, Schmitt LM, Dominick KC, Shaffer RC, et al. Sex differences in resting EEG power in Fragile X Syndrome. J Psychiatr Res. 2021;138: 89–95.

84. Llinas RR, Ribary U, Jeanmonod D, Kronberg E, Mitra PP. Thalamocortical dysrhythmia: A neurological and neuropsychiatric syndrome characterized by magnetoencephalography. Proc Natl Acad Sci U S A. 1999;96: 15222–15227.

85. Wöstmann M, Waschke L, Obleser J. Prestimulus neural alpha power predicts confidence in discriminating identical auditory stimuli. Eur J Neurosci. 2019;49: 94–105.

86. Strauß A, Wöstmann M, Obleser J. Cortical alpha oscillations as a tool for auditory selective inhibition. Front Hum Neurosci. 2014;8. doi:10.3389/fnhum.2014.00350

87. Wöstmann M, Lim SJ, Obleser J. The Human Neural Alpha Response to Speech is a Proxy of Attentional Control. Cereb Cortex. 2017;27: 3307–3317.

88. Klimesch W, Sauseng P, Hanslmayr S. EEG alpha oscillations: the inhibition-timing hypothesis. Brain Res Rev. 2007;53: 63–88.

89. Stropahl M, Bauer A-KR, Debener S, Bleichner MG. Source-Modeling Auditory Processes of EEG Data Using EEGLAB and Brainstorm. Front Neurosci. 2018;12. doi:10.3389/fnins.2018.00309

90. Sahin M, Jones SR, Sweeney JA, Berry-Kravis E, Connors BW, Ewen JB, et al.

Discovering translational biomarkers in neurodevelopmental disorders. Nat Rev Drug Discov. England; 2018.

91. Norris JE, DeStefano LA, Schmitt LM, Pedapati EV, Erickson CA, Sweeney JA, Ethridge LE. Hemispheric Utilization of Alpha Oscillatory Dynamics as a Unique Biomarker of Neural Compensation in Females with Fragile X Syndrome. ACS Chem Neurosci. 2022 Dec 7;13(23):3389-3402. doi: 10.1021/acschemneuro.2c00404.

Supporting Information

Supplementary Table 1. Assignment of cortical nodes to region groupings as attributed by the Desikan-Killiany (DK) atlas.

			MNI Centroid			
Node	Abbreviation	Cortex	x	y	z	Vert.
Caudal Anterior Cingulate R	cACC R	RL	4	22	27	68
Isthmus Cingulate L	iCC L	LL	-7	-45	18	81
Isthmus Cingulate R	iCC R	RL	6	-42	19	91
Lateral Orbitofrontal L	LOF L	LPF	-25	30	-19	221
Lateral Orbitofrontal R	LOF R	RPF	23	32	-19	206
Medial Orbitofrontal L	MOF L	LPF	-7	33	-17	155
Medial Orbitofrontal R	MOF R	RPF	4	37	-15	170
Parahippocampal L	paraH L	LT	-26	-29	-21	68
Parahippocampal R	paraH R	RT	24	-30	-19	66
Posterior Cingulate L	PCC L	LL	-5	-15	38	85
Posterior Cingulate R	PCC R	RL	5	-17	39	93
Precuneus L	PCUN L	LP	-9	-59	38	314
Precuneus R	PCUN R	RP	10	-58	38	325
Rostral Anterior Cingulate L	rACC L	LL	-5	39	1	78
Rostral Anterior Cingulate R	rACC R	RL	4	38	3	56
Caudal Middle Frontal L	cMFG L	LF	-37	11	47	224
Caudal Middle Frontal R	cMFG R	RF	37	13	48	186
Insula L	INS L	LT	-38	-2	2	174
Insula R	INS R	RT	36	2	-2	196
Rostral Middle Frontal L	rMFG L	LF	-34	47	17	543
Rostral Middle Frontal R	rMFG R	RF	34	48	17	551
Supramarginal L	SMAR L	LP	-57	-38	34	305
Supramarginal R	SMAR R	RP	54	-31	36	302
Caudal Anterior Cingulate L	cACC L	LL	-5	21	26	48
Inferior Temporal L	ITG L	LT	-53	-36	-22	307
Inferior Temporal R	ITG R	RT	51	-32	-25	316
Middle Temporal L	MTG L	LT	-58	-23	-15	277
Middle Temporal R	MTG R	RT	58	-22	-15	324
Pars Opercularis L	pOPER L	LF	-49	17	14	139
Pars Opercularis R	pOPER R	RF	49	17	14	118
Pars Orbitalis L	pORB L	LPF	-44	39	-14	72
Pars Orbitalis R	pORB R	RPF	43	42	-15	68
Pars Triangularis L	pTRI L	LF	-47	32	1	101
Pars Triangularis R	pTRI R	RF	48	34	2	148

Superior Temporal L	STG L	LT	-55	-12	-4	290
Superior Temporal R	STG R	RT	54	-6	-7	257
Cuneus L	CUN L	LO	-6	-80	19	93
Cuneus R	CUN R	RO	8	-78	20	99
Fusiform L	FUS L	LT	-36	-43	-22	268
Fusiform R	FUS R	RT	35	-41	-23	255
Lateral Occipital L	LOG L	LO	-31	-89	0	371
Lateral Occipital R	LOG R	RO	35	-85	2	367
Lingula L	LING L	LO	-14	-71	-5	246
Lingula R	LING R	RO	13	-67	-4	227
Banks of Sup. Temp. Sulcus L	BSTS L	LT	-53	-45	8	76
Banks of Sup. Temp. Sulcus R	BSTS R	RT	54	-41	10	70
Entorhinal L	ENT L	LT	-26	-5	-33	30
Entorhinal R	ENT R	RT	23	-6	-35	32
Frontal Pole L	FP L	LPF	-7	68	-11	22
Frontal Pole R	FP R	RPF	7	68	-15	30
Inferior Parietal L	IPL L	LP	-42	-71	32	351
Inferior Parietal R	IPL R	RP	46	-63	32	421
Paracentral L	paraC L	LC	-7	-30	57	110
Paracentral R	paraC R	RC	7	-27	57	128
Pericalcarine L	periCAL L	LO	-11	-82	6	109
Pericalcarine R	periCAL R	RO	12	-80	7	110
Postcentral L	postC L	LC	-46	-22	45	333
Postcentral R	postC R	RC	44	-20	46	307
Precentral L	preC L	LC	-41	-9	46	339
Precentral R	preC R	RC	40	-7	46	353
Superior Frontal L	sFG L	LF	-12	30	41	671
Superior Frontal R	sFG R	RF	12	32	41	603
Superior Parietal L	SPL L	LP	-23	-65	50	484
Superior Parietal R	SPL R	RP	24	-65	51	464
Temporal Pole L	TP L	LT	-28	14	-38	38
Temporal Pole R	TP R	RT	27	16	-36	38
Transverse Temporal L	TT L	LT	-46	-23	10	34
Transverse Temporal R	TT R	RT	46	-17	9	23

898 The MNI coordinates and number of vertices included in each node parcel are also displayed. We
899 considered nodes as replicates within regions within our linear models. Abbreviations: L, Left; R,
900 right; F, frontal; L, cingulate; O, occipital; P, parietal; PF, prefrontal; T, temporal; MNI, Montreal
901 Neurologic Institute; Vert., Number of Vertices.

902 **Supplementary Table 2: Summary of linear mixed model results.**

Model	Predictor	numDF	denDF	F-value	p-value
ITC: 40 Hz	(Intercept)	1	4,973	16987.5	<.001
	group	1	71	6.9	.011
	sex	1	71	3e-04	.986
	region	13	4,973	38.9	<.001
	group:sex	1	71	3.9	.053
	group:region	13	4,973	1.5	.124
	sex:region	13	4,973	1.7	.058
	group:sex:region	13	4,973	1.9	.025
ITC: 80 Hz	(Intercept)	1	4,973	16135.3	<.001
	group	1	71	3.9	.053
	sex	1	71	.8	.367
	region	13	4,973	15.2	<.001
	group:sex	1	71	.6	.456
	group:region	13	4,973	4.6	<.001
	sex:region	13	4,973	1.5	.121
	group:sex:region	13	4,973	1.2	.242
ITC: Onset	(Intercept)	1	4,973	7853.2	<.001
	group	1	71	4.3	.042
	sex	1	71	.01	.936
	region	13	4,973	51.9	<.001
	group:sex	1	71	.1	.728
	group:region	13	4,973	2.9	<.001
	sex:region	13	4,973	2.8	<.001
	group:sex:region	13	4,973	1.4	.142
ITC: Offset	(Intercept)	1	4,973	14939.9	<.001
	group	1	71	1.5	.218
	sex	1	71	.01	.922
	region	13	4,973	21.8	<.001
	group:sex	1	71	.1	.783
	group:region	13	4,973	1.7	.062
	sex:region	13	4,973	.9	.568
	group:sex:region	13	4,973	1.7	.047
STP: Gamma1	(Intercept)	1	4,973	1530204.9	<.001
	group	1	71	12.7	<.001
	sex	1	71	36.4	<.001
	region	13	4,973	434.0	<.001
	group:sex	1	71	4.2	.045
	group:region	13	4,973	2.6	.002
	sex:region	13	4,973	2.6	.001
	group:sex:region	13	4,973	.7	.799
STP: Gamm2	(Intercept)	1	4,973	971679.6	<.001

	group	1	71	1.4	.235
	sex	1	71	13.7	<.001
	region	13	4,973	461.9	<.001
	group:sex	1	71	7.8	.007
	group:region	13	4,973	2.5	.002
	sex:region	13	4,973	2.3	.006
	group:sex:region	13	4,973	.5	.943
STP: Alpha	(Intercept)	1	4,973	684410.9	<.001
	group	1	71	4.0	.048
	sex	1	71	1.7	.190
	region	13	4,973	171.5	<.001
	group:sex	1	71	6.4	.014
	group:region	13	4,973	2.8	<.001
	sex:region	13	4,973	5.5	<.001
	group:sex:region	13	4,973	9.6	<.001
ERSP: Gamma1	(Intercept)	1	4,973	8.2	.004
	group	1	71	2.4	.123
	sex	1	71	3.9	.052
	region	13	4,973	2.1	.011
	group:sex	1	71	.03	.866
	group:region	13	4,973	1.5	.122
	sex:region	13	4,973	.8	.663
	group:sex:region	13	4,973	2.7	<.001
ERSP: Gamma2	(Intercept)	1	4,973	4.9	.027
	group	1	71	1.0	.330
	sex	1	71	3.7	.059
	region	13	4,973	2.5	.002
	group:sex	1	71	.2	.659
	group:region	13	4,973	2.7	<.001
	sex:region	13	4,973	2.4	.004
	group:sex:region	13	4,973	2.0	.017
ERSP: Alpha	(Intercept)	1	4,973	13.7	<.001
	group	1	71	1.3	.251
	sex	1	71	3.1	.081
	region	13	4,973	6.2	<.001
	group:sex	1	71	6.1	.016
	group:region	13	4,973	1.6	.079
	sex:region	13	4,973	1.0	.403
	group:sex:region	13	4,973	2.8	<.001

903 A series of linear mixed-effects models (LME) were conducted for each of the ten power and
904 phase response variables (see Methods). To account for individual variation in electrode position,

905 we opted to perform statistical modeling at the region level and use nodes within a region as
906 replicates. Fixed effects included Group (FXS or TDC), Sex (male or female), and Region (14).

907 **Supplementary Figure 1: Broadband auditory chirp stimulus.**

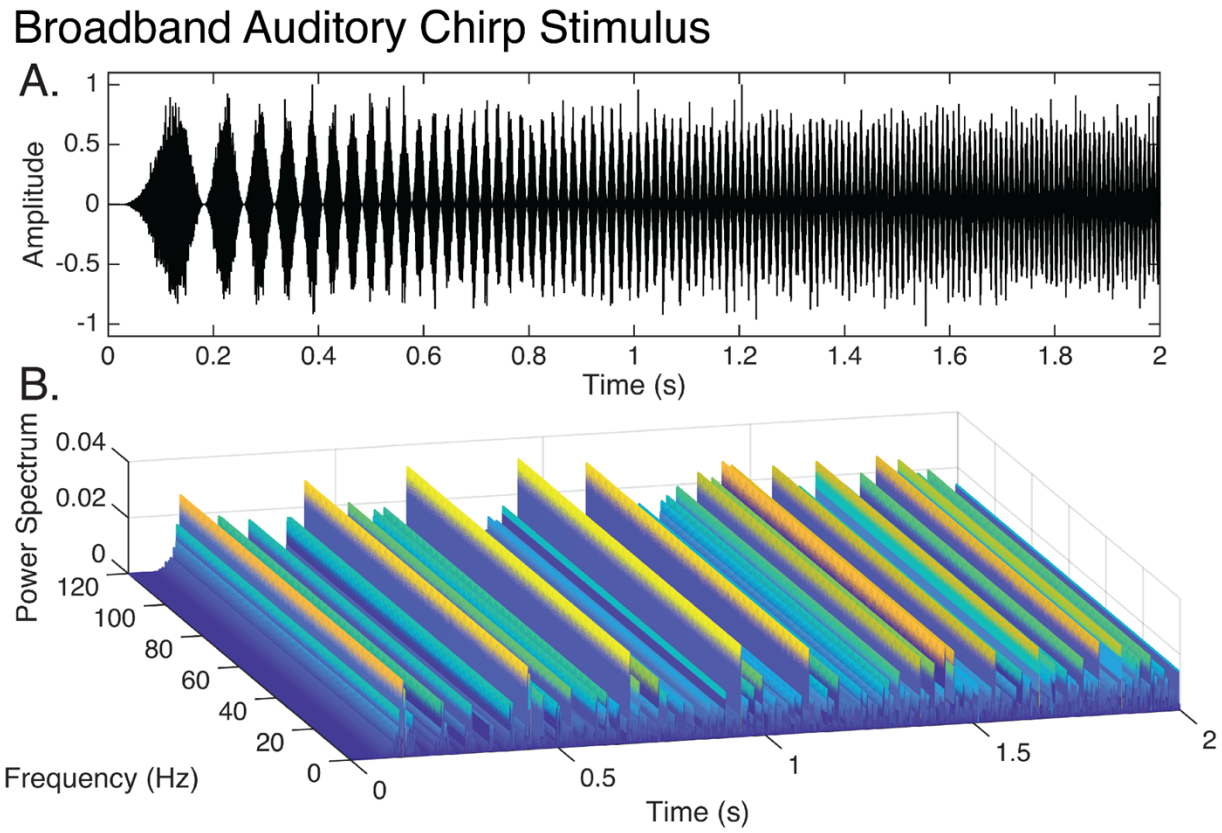

908

909 **Supplementary Figure 1:** A. Plot of amplitude-modulated pink noise carrier waveform.

910 Frequency of modulation increases linearly from 0 to 120 Hz over 2 seconds. B. Waterfall plot

911 depicting broadband power spectrum of broadband chirp stimulus.

912

913 **Supplementary Figure 2: Atlas Regions**

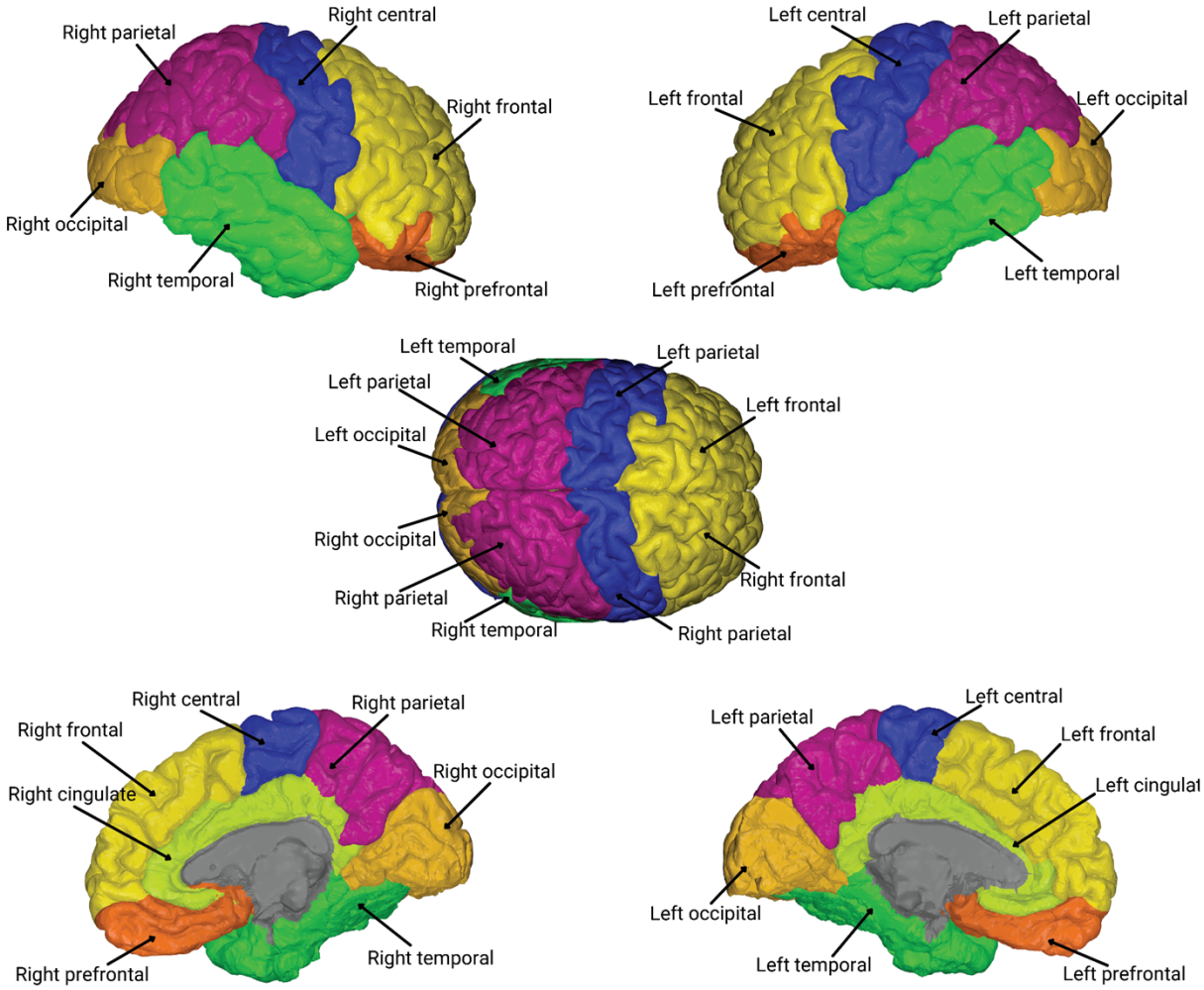

914

915 **Supplementary Figure 2:** The Desikan-Killiany atlas was used to group vertex parcellations
916 following source localization. A total of 14 hierarchical regions (shown below) encompass 68
917 cortical nodes as described in Supplemental Table 1.

Supplementary Figure 3: Frontotemporal atlas nodes for transfer entropy estimation

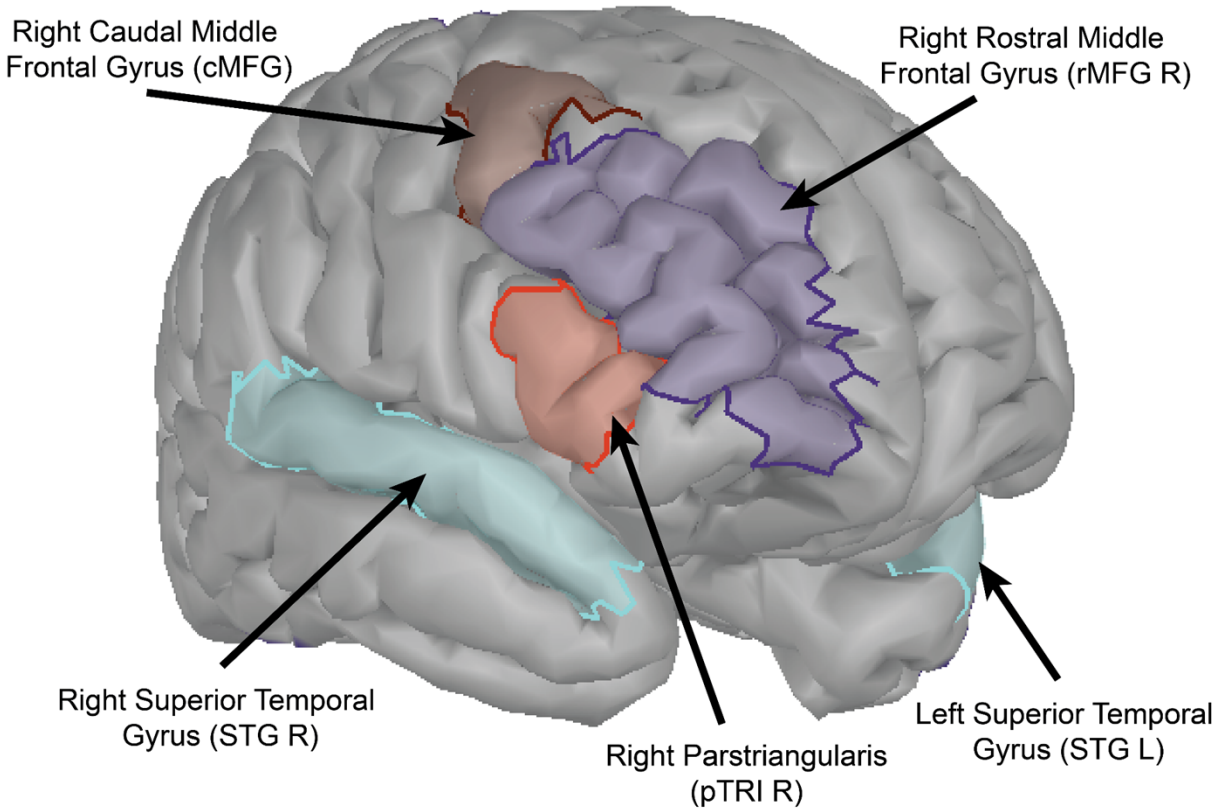

Supplementary Figure 3: Transfer entropy was calculated between frontotemporal nodes associated with significant group differences in onset and gamma ITPC. Onset ITPC was significantly increased within the caudal middle frontal R (cMFG; t=2.73, p=.001), pars triangularis R (pTRI, t =2.69, p=.011), and rostral middle frontal R (rMFG; t=2.44, p=.019) in FXS. Renyi transfer entropy was estimated between these frontal nodes and right and left superior temporal gyrus (STG), which is the node-level region that includes the auditory cortex.